Supplementary Information

N, N′, N″-tris(4-acetyl-aniline)

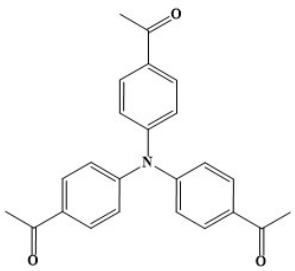

A solution of acetyl chloride (1.12g, 15mmol) and anhydrous aluminum chloride (1.12 g, 15mmol) in dry DCM (dichloromethane) was stirred for 15 minutes. In a nitrogen atmosphere, the mixture was slowly dripped into the DCM (80ml) solution of triphenylamine (1.22g, 5mmol), reaction for 12 hours under the condition of 273－278 K, after that, heated to 313K and continue to react for 12 hours, the resulting mixture was carefully quenched with ethyl alcohol. the organic solvents were evaporated in vacuo. The crude product was extracted three times by DCM, after that, combined organic extract and dried over MgSO4. The pure product was obtained by silica gel column chromatography, Yield 1.37 g (73.85 %); ^{1}H NMR (400 MHz, $CDCl_3$, 298K, ppm) δ = 2.60 (s, 9H), 7.18–7.16 (d, 6H), 7.93-7.91 (d, 6H).

N, N′, N″-tris[4-(4,4,4-trifluoro-1,3-dioxobutyl)-aniline],

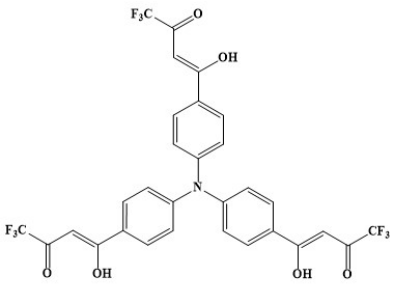

A mixture of sodium ethoxide, (1.09 g, 16.0mmol) N, N′, N″-tris(4-acetyl-aniline) (1.85 g, 5 mmol) and ethyl trifluoroacetate (2.30 g, 16.2 mmol) in 30 mL ethyl alcohol. Then, reaction for 12 hours under the condition of ice water bath. The resulting solution was acidified to pH 3-4 using hydrochloric acid (1 M solution). The

crude product was extracted three times by EA (ethyl acetate), combined organic extract and dried over $MgSO_4$. Recrystallization with acetonitrile, yellow needle crystals were filtered and dried in vacuum, Yield 2.02 g (61.30 %); ^{1}H NMR ($CDCl_3$, 400 MHz, 298K, ppm): δ = 15.41 (s, 3H), 7.96–7.95 (d, 6H), 7.23–7.21 (d, 6H), 6.54 (s, 3H).

Tris(4-(5-(trifluoromethyl)-1*H*-pyrazol-3-yl) phenyl) amine, H_3L

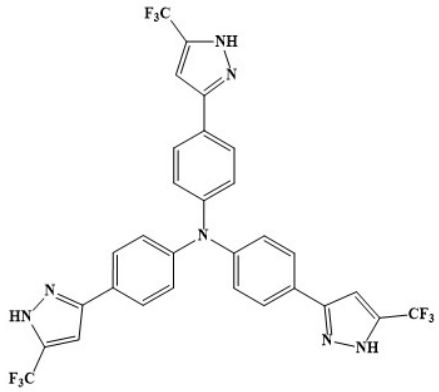

A mixture of hydrazine hydrate, (1.30 g, 25.0mmol) and N, N′, N″-tris[4-(4,4,4-trifluoro-1,3-dioxobutyl)-aniline] (1.65g, 2.5mmol) in 30 mL methyl alcohol. reaction for 12 hours under the condition of 333 K, after that, yellow precipitate was filtered and dried in vacuum, Yield 1.50g (92.76 %); ^{1}H NMR (DMSO, 400 MHz, 298K, ppm): δ = 7.14 (s, 3H), 7.18–7.16 (d, 6H), 7.79–7.81 (d, 6H). ^{13}C NMR (100 MHz, DMSO, 298K, ppm): δ 147.30, 144.14, 127.49, 124.73, 123.59, 120.92, 101.02.

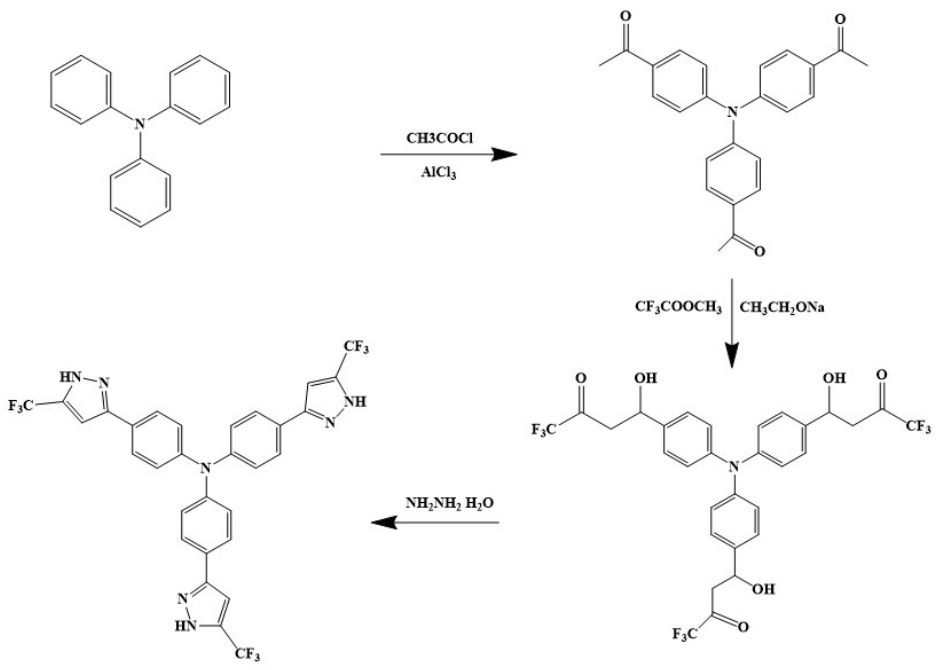

Fig. S1 Synthetic route of **H_3L**.

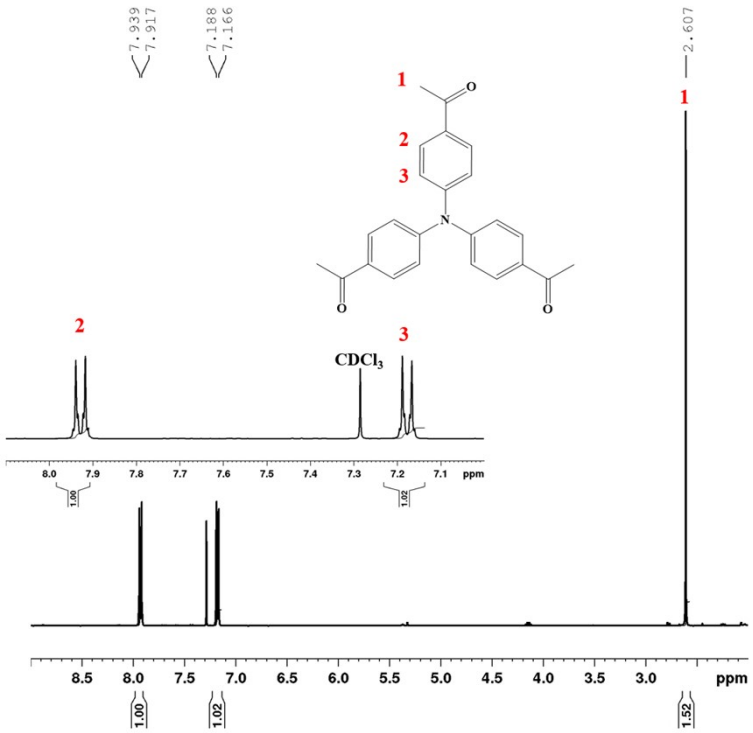

Fig. S2 ^{1}H NMR spectrum of N, N′, N″-tris(4-acetyl-aniline) in $CDCl_3$.

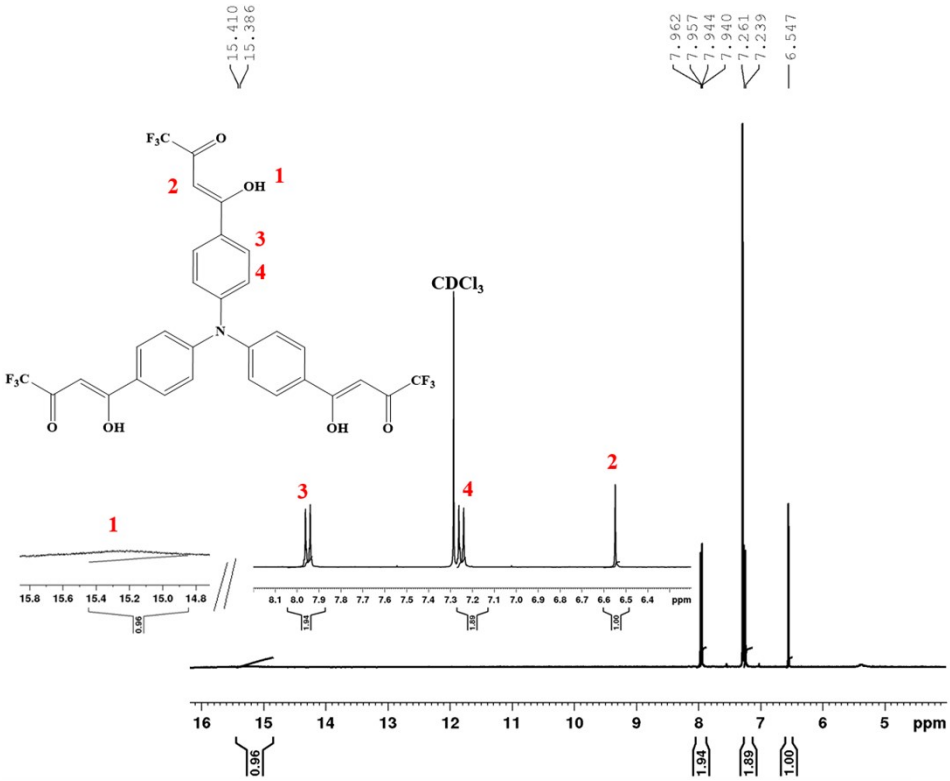

Fig. S3 ^{1}H NMR spectrum of N, N′, N″-tris[4-(4,4,4-trifluoro-1,3-dioxobutyl)-aniline] in $CDCl_3$.

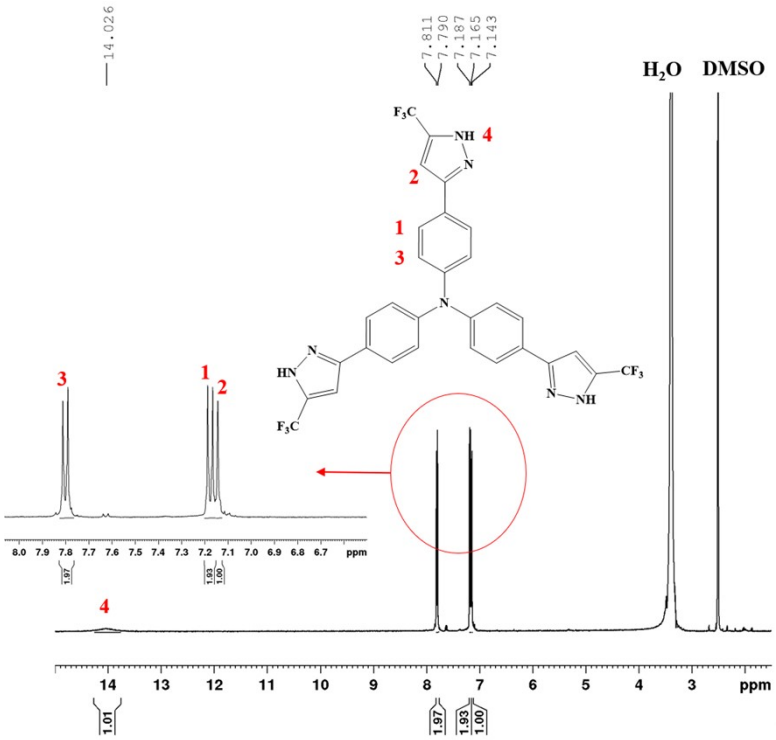

Fig. S4 ^{1}H NMR spectrum of **H_3L** in DMSO-d_6.

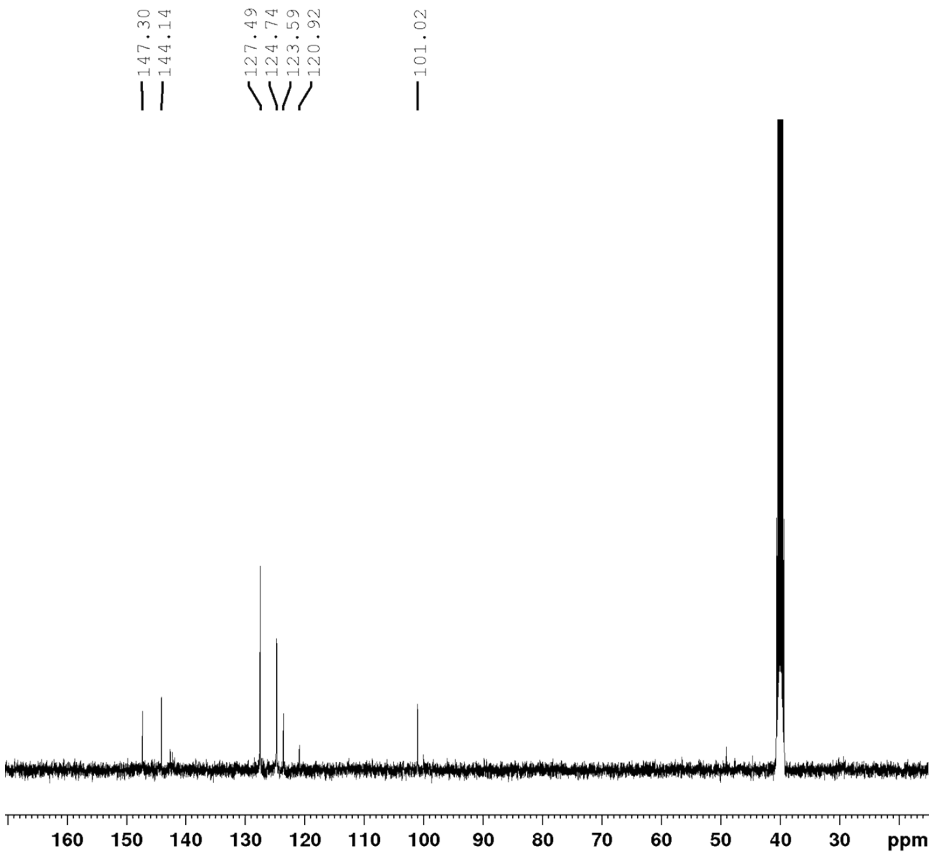

Fig. S5 ^{13}C NMR spectrum of $\mathbf{H_3L}$ in DMSO-d_6.

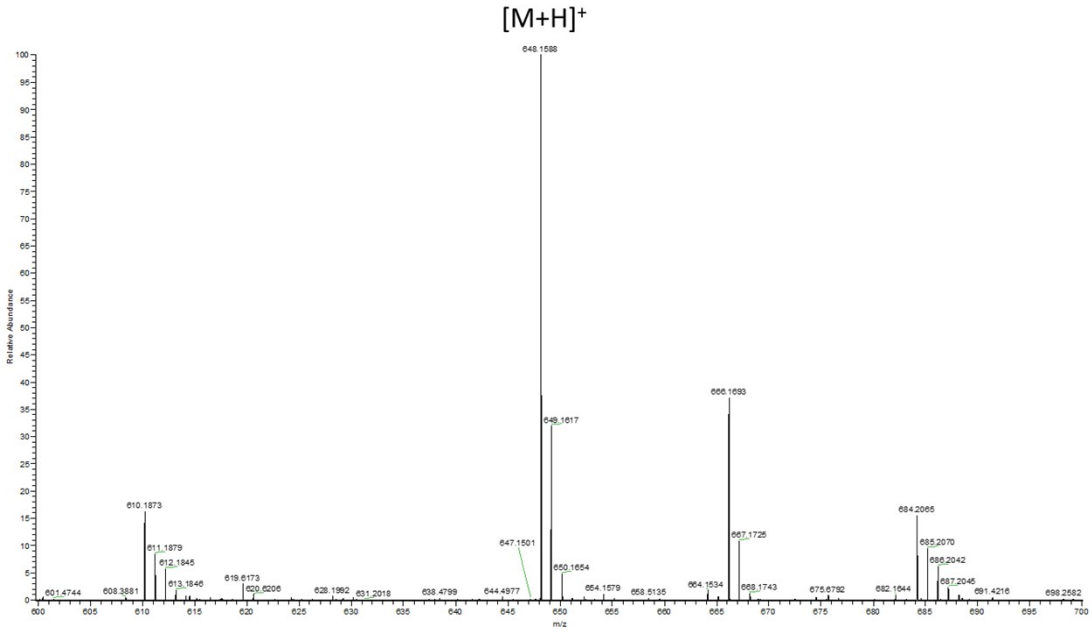

Fig. S6 ESI-MS of $\mathbf{H_3L}$ in CH_3CN.

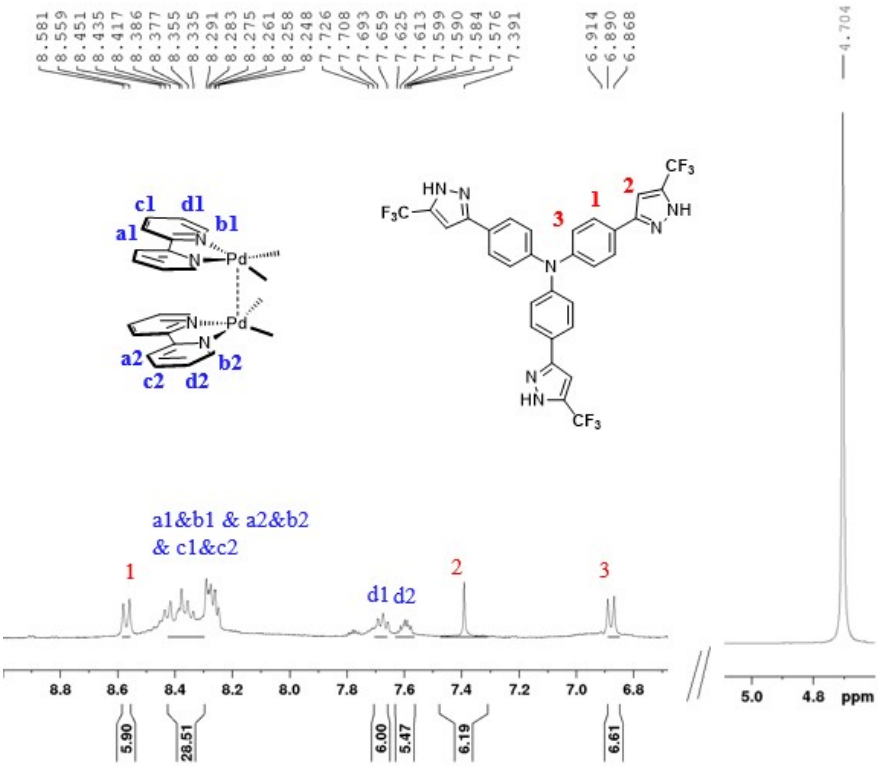

Fig. S7 The ^{1}H NMR spectrum of **1** in D_2O at 298 K.

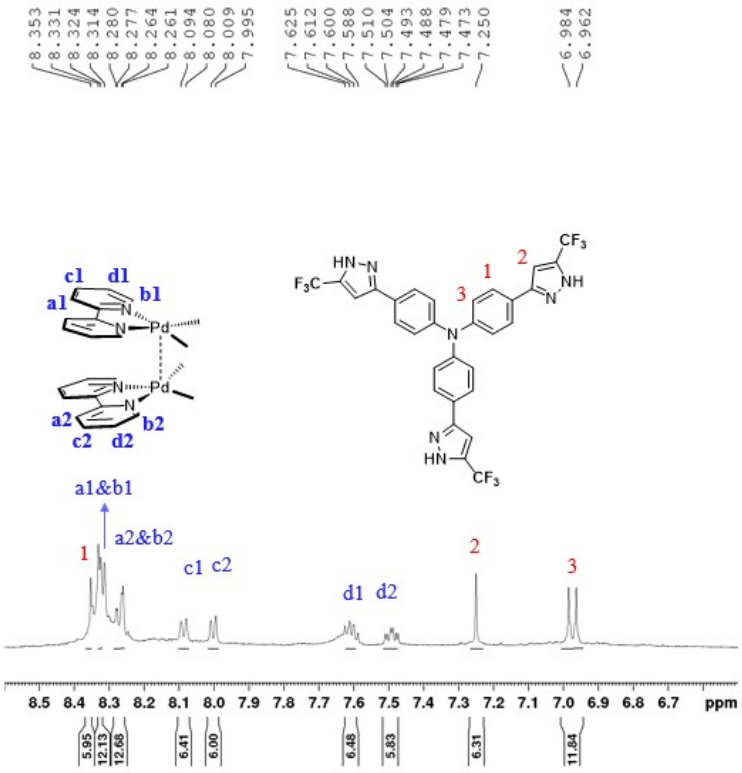

Fig. S8 The ^{1}H NMR spectrum of **1a** in CD_3CN at 298 K.

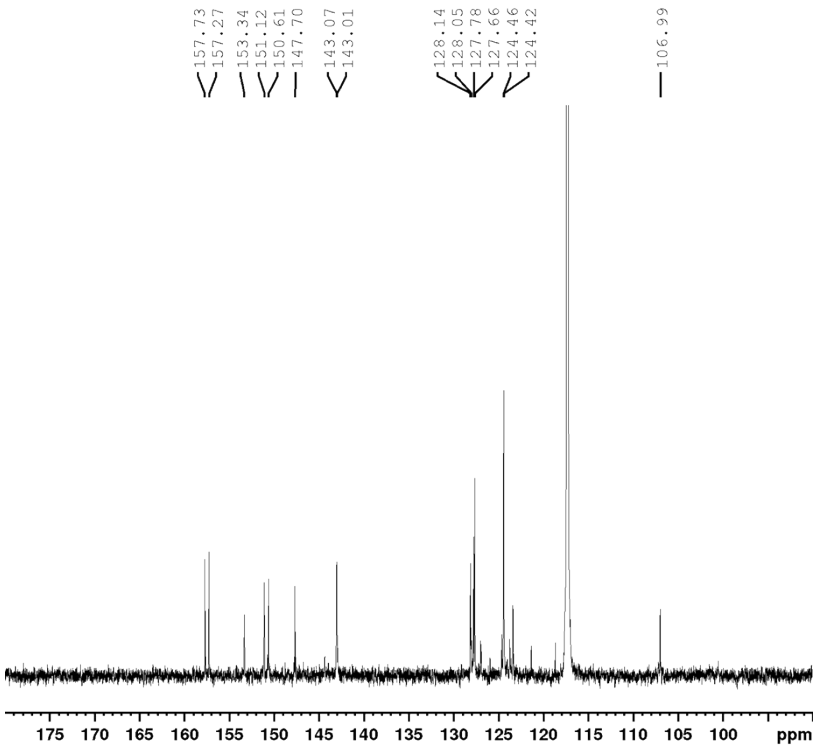

Fig. S9 The ^{13}C NMR spectrum of **1a** in CD_3CN at 298 K.

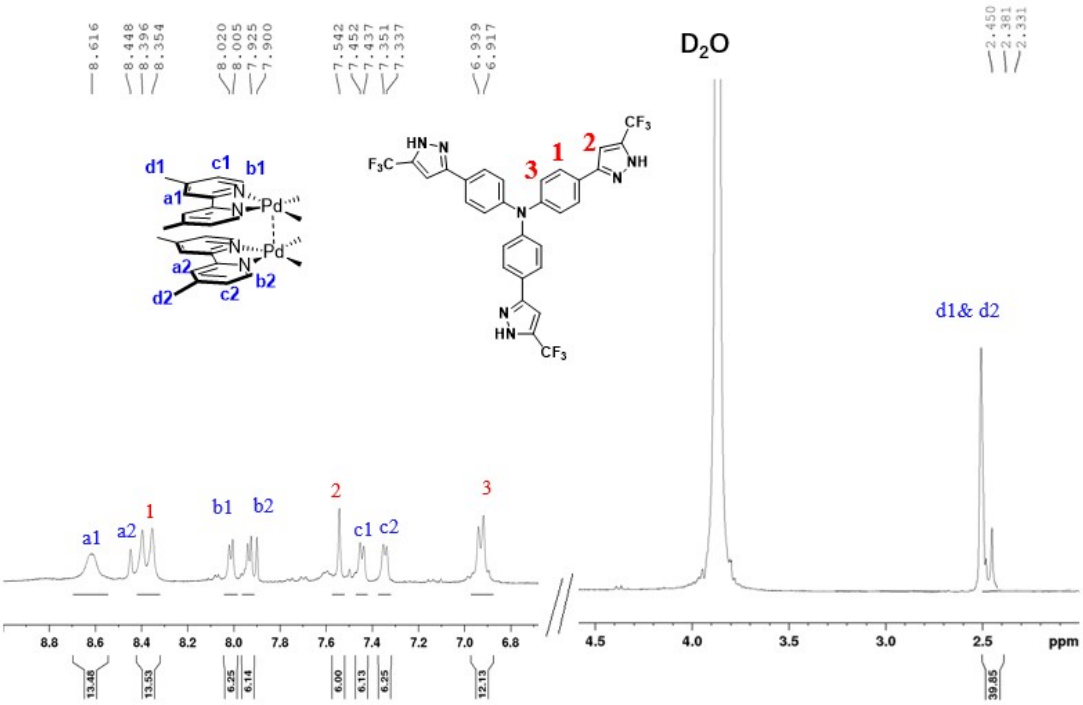

Fig. S10 The ^{1}H NMR spectrum of **2** in D_2O at 298 K.

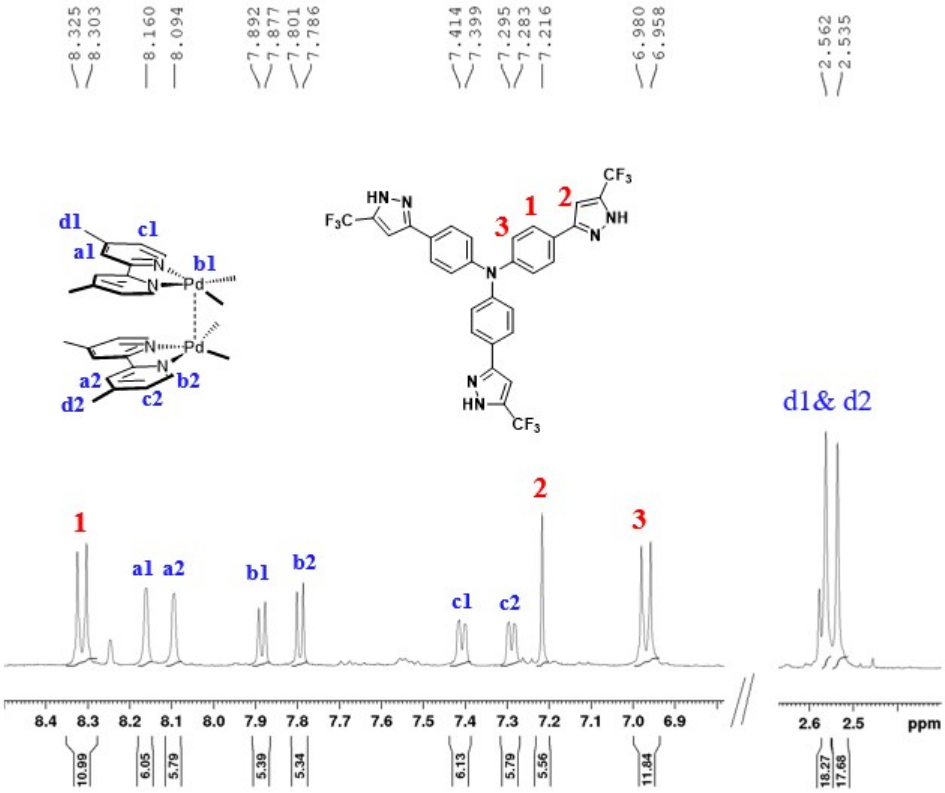

Fig. S11 The ^{1}H NMR spectrum of **2a** in CD_3CN at 298 K.

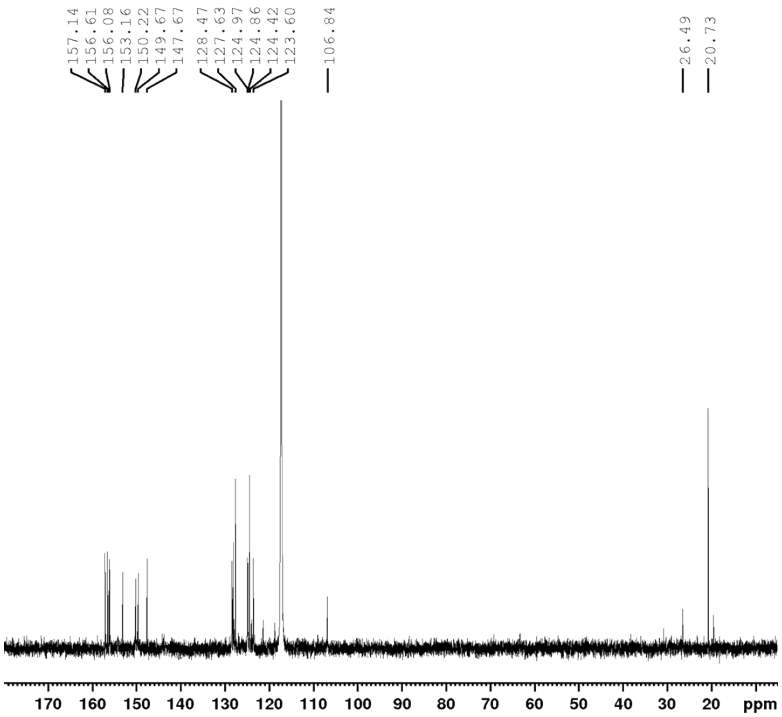

Fig. S12 The ^{13}C NMR spectrum of **2a** in CD_3CN at 298 K.

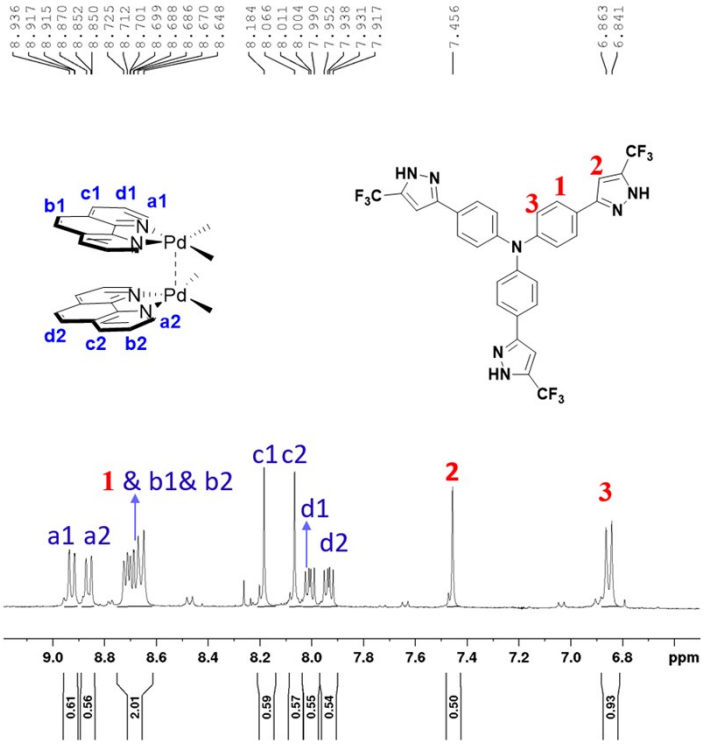

Fig. S13 The ^{1}H NMR spectrum of **3** in D_2O at 298 K.

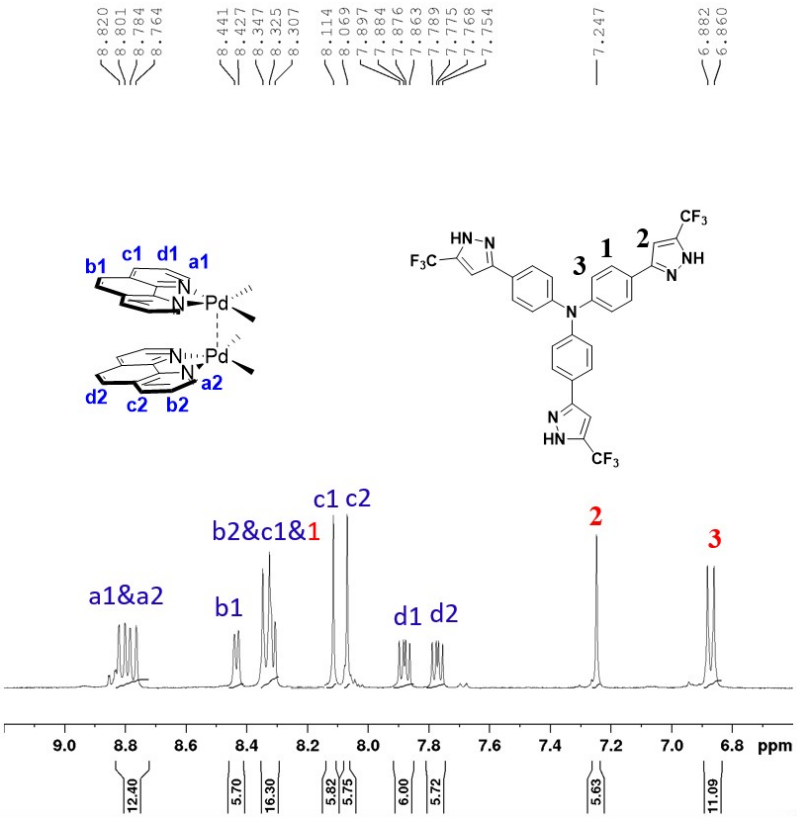

Fig. S14 The ^{1}H NMR spectrum of **3a** in CD_3CN at 298 K.

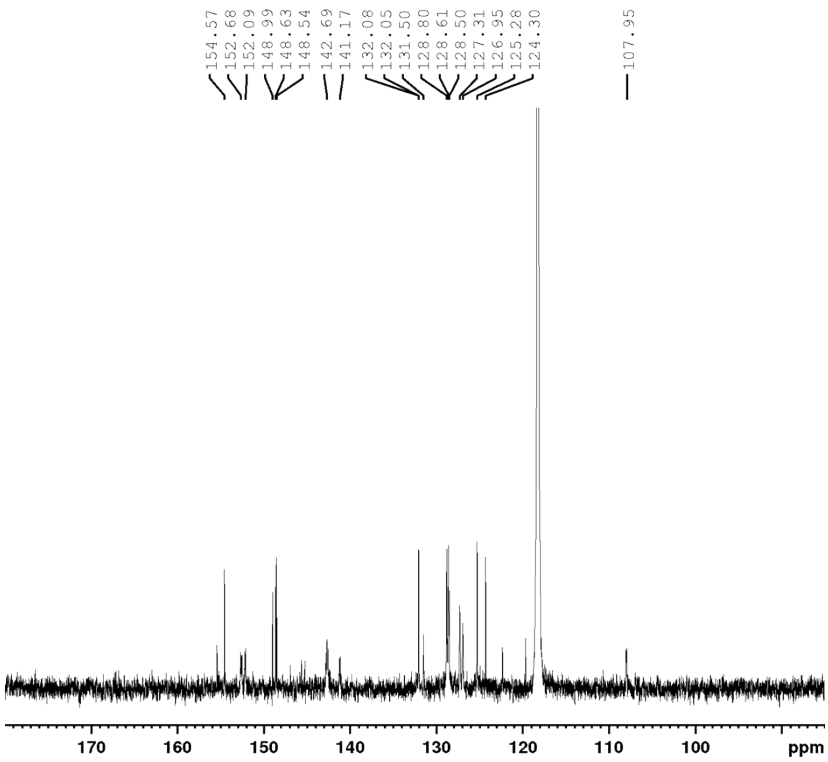

Fig. S15 The ^{13}C NMR spectrum of **3a** in CD_3CN at 298 K.

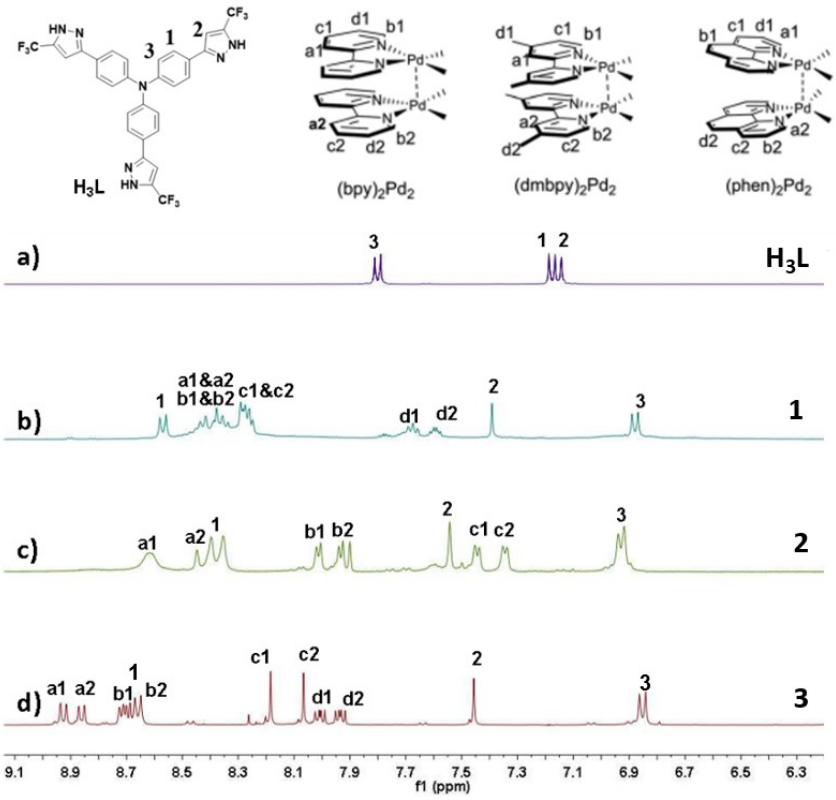

Fig. S16 The ^{1}H NMR spectra of H_3L (a), **1** (b), **2** (c), **3** (d) in D_2O at 298K.

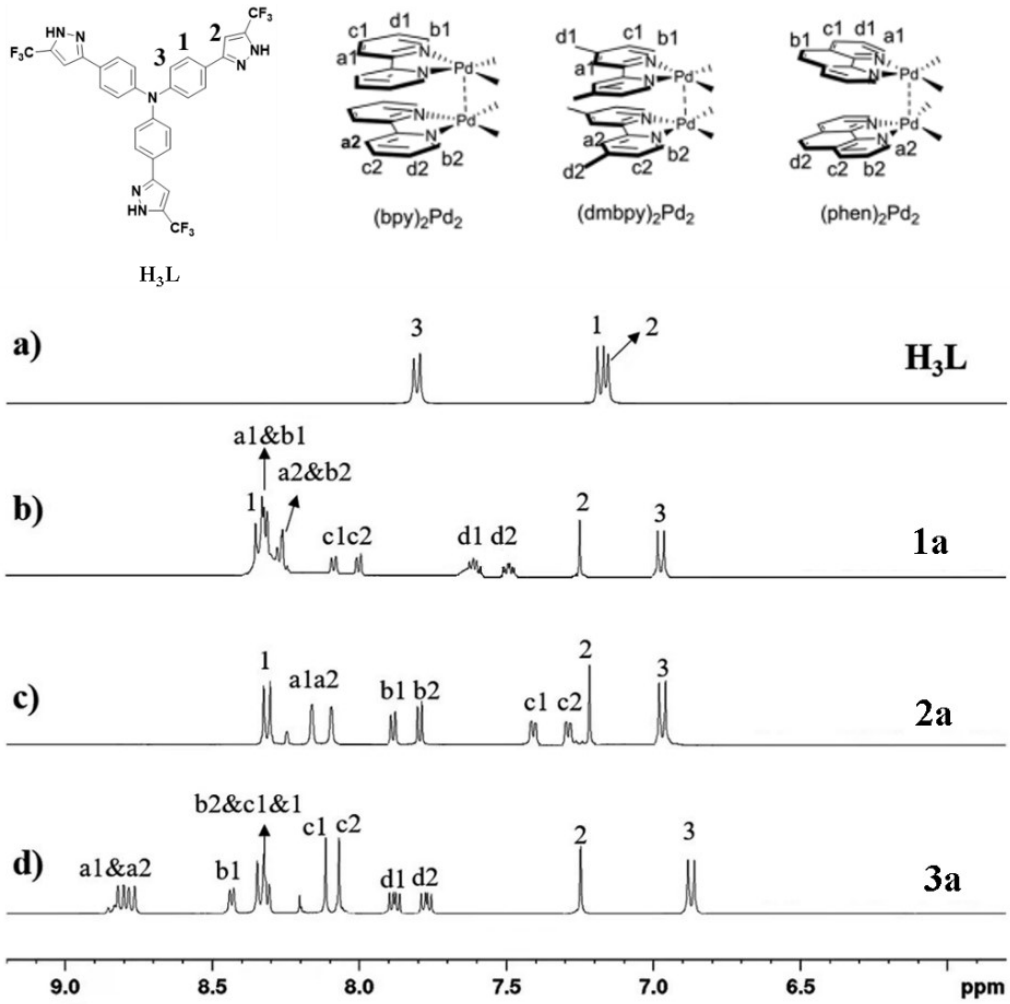

Fig. S17 The ^{1}H NMR spectra of H_3L (a), **1a** (b), **2a** (c), **3a** (d) in CD_3CN at 298K.

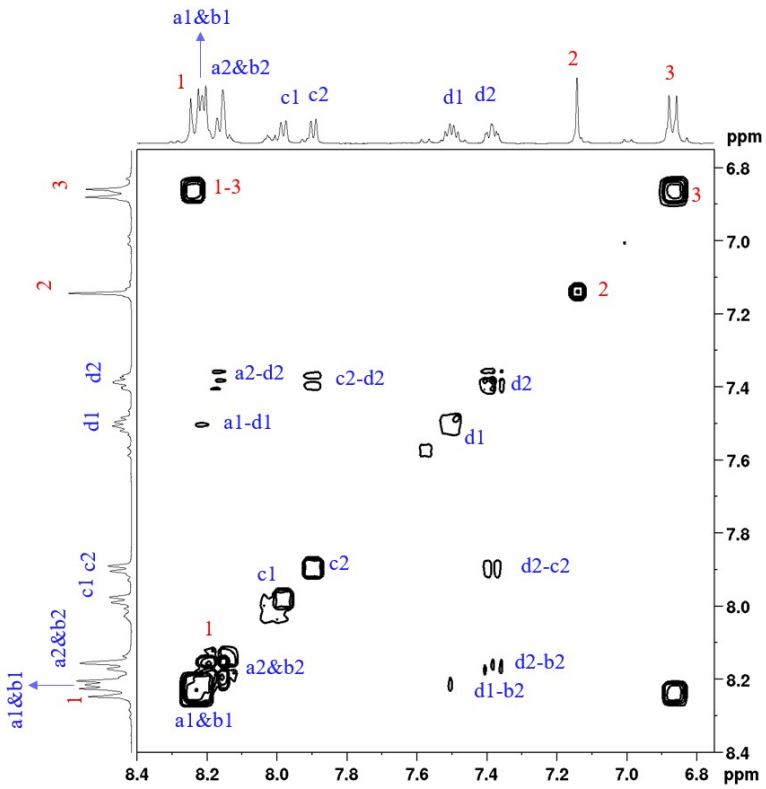

Fig. S18 ^{1}H-^{1}H COSY spectrum of **1a** in CD_3CN at 298 K.

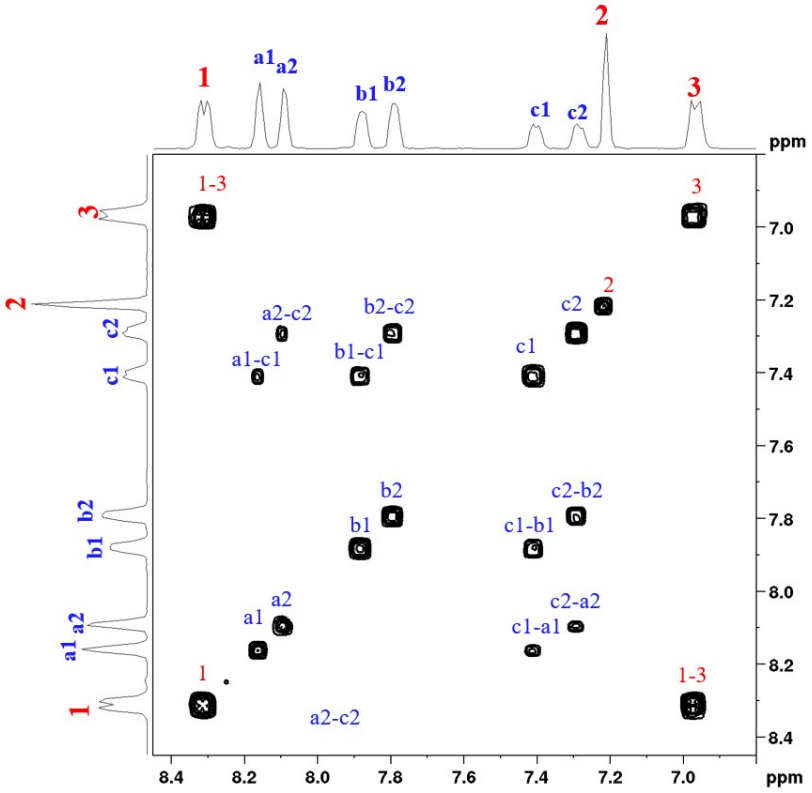

Fig. S19 ^{1}H-^{1}H COSY spectrum of **2**a in CD_3CN at 298 K.

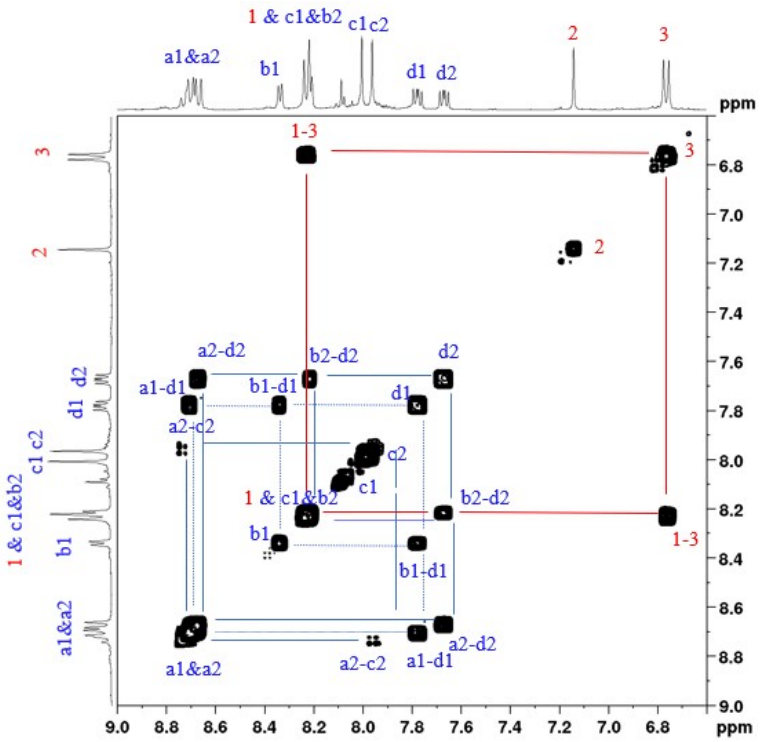

Fig. S20 ^{1}H-^{1}H COSY spectrum of **3**a in CD_3CN at 298 K.

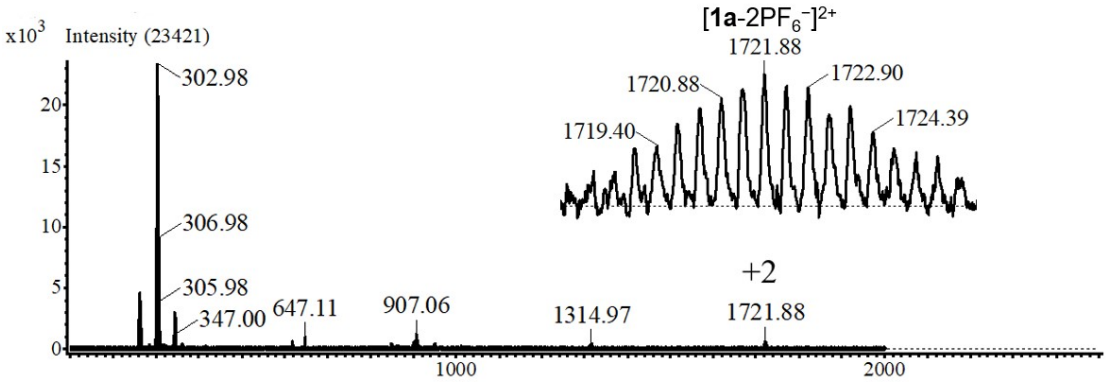

Fig. S21 ESI-MS spectra of **1a** in CH_3CN; the inset shows the isotopic distribution of the species [**1a**-2PF_6^-]$^{2+}$. (cal. 1720.78)

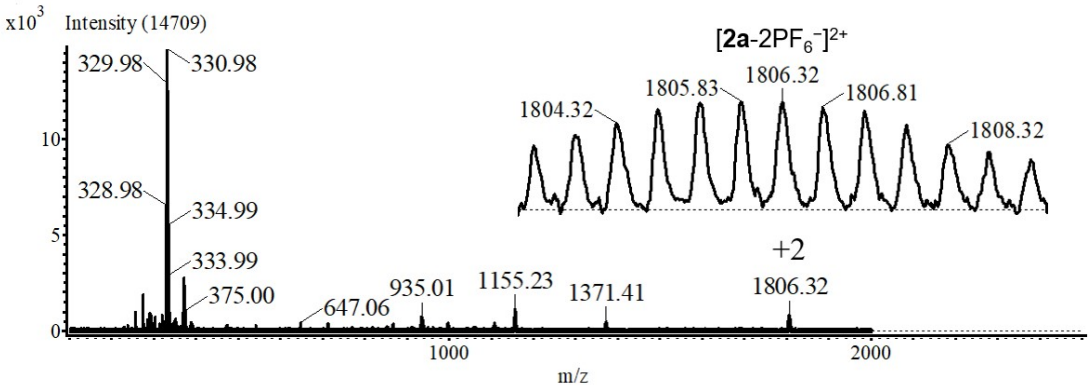

Fig. S22 ESI-MS spectra of **2a** in CH_3CN; the inset shows the isotopic distribution of the species [**2a**-$2PF_6^-$]$^{2+}$. (cal. 1801.78)

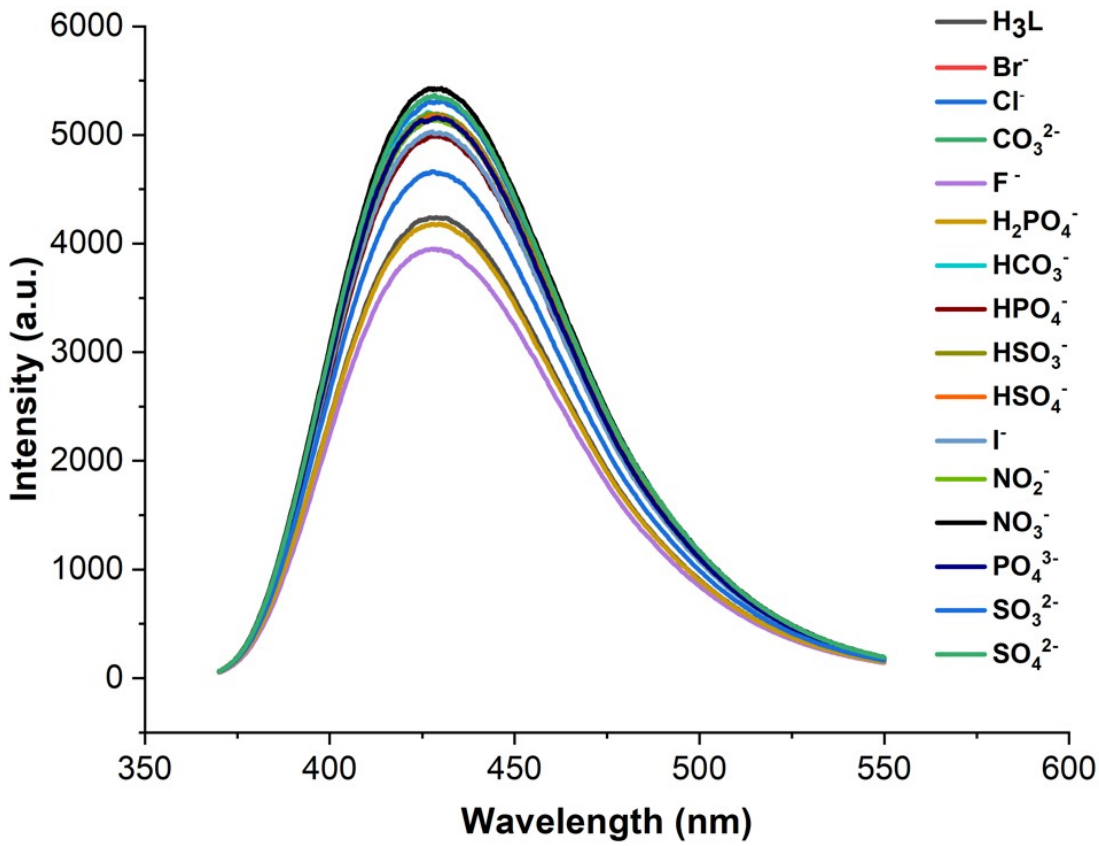

Fig. S23 Changes in fluorescent intensity for **H_3L** (1.0×10^{-5} M) in CH_3CN/H_2O (1:2, v/v) upon addition of different anions (Na^+ salts in H_2O).

Fig. S24 PL emission photograph of **1a**, **2a** and **3a** before and after addition of HSO_3^-.

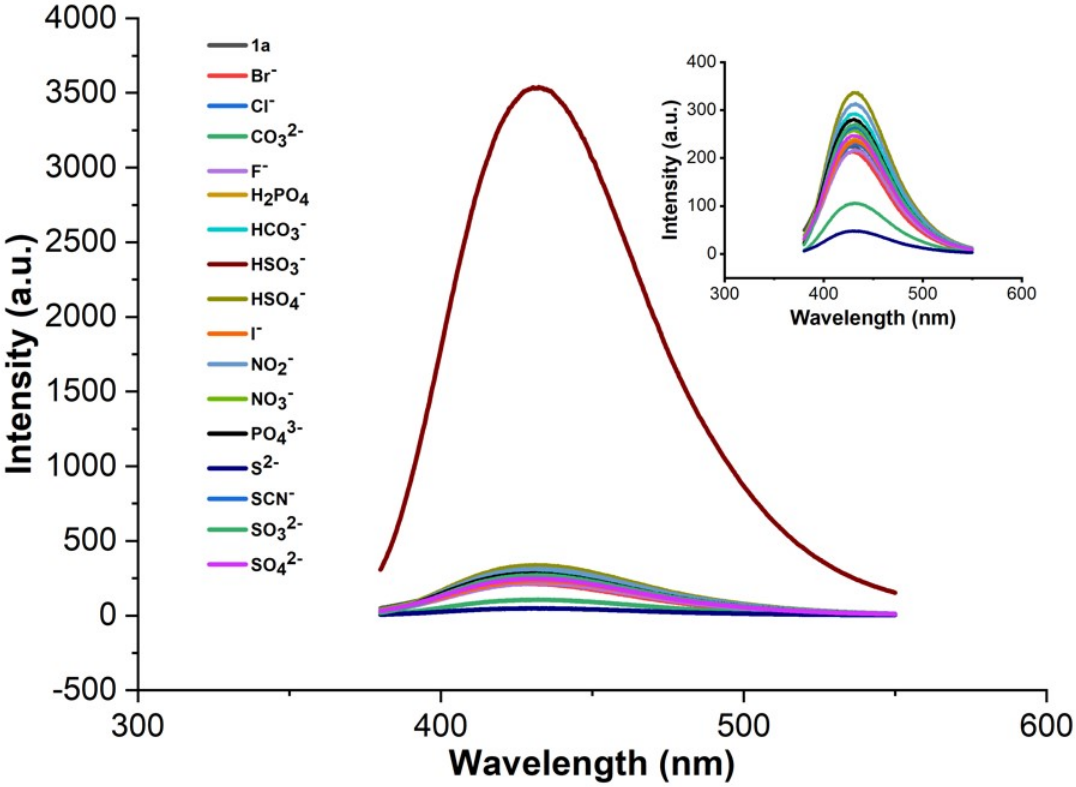

Fig. S25 Changes in fluorescent intensity for **1a** (1.0×10^{-5} M) in CH_3CN/H_2O (1:2, v/v) upon addition of different anions (Na^+ salts in H_2O).

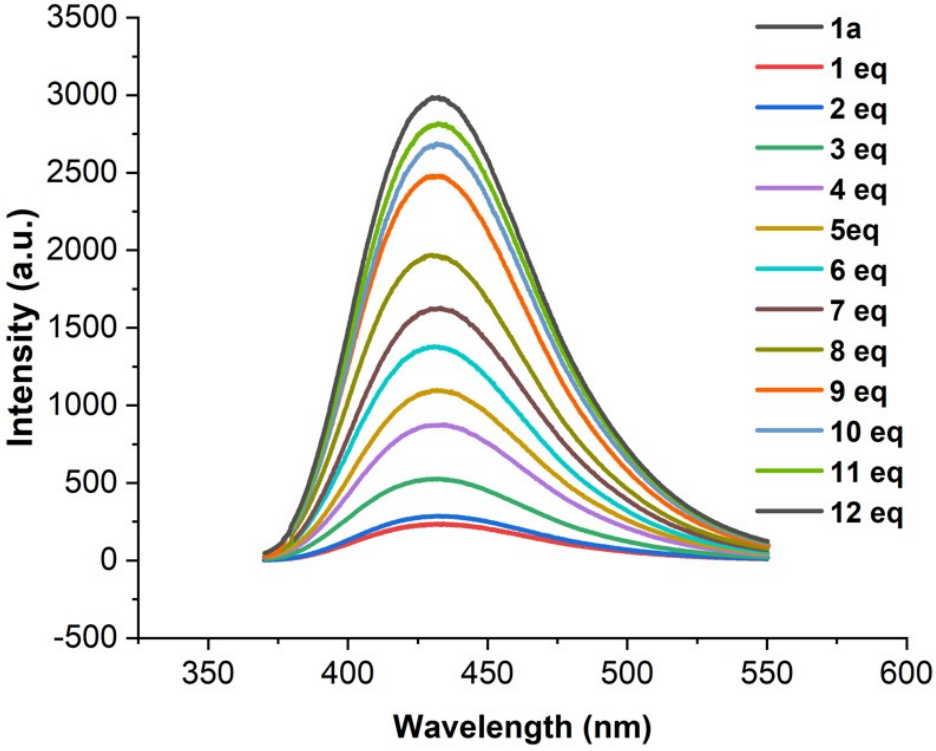

Fig. S26 Fluorescence spectra of **1a** in CH_3CN/H_2O (1:2, v/v) for various concentrations of HSO_3^-.

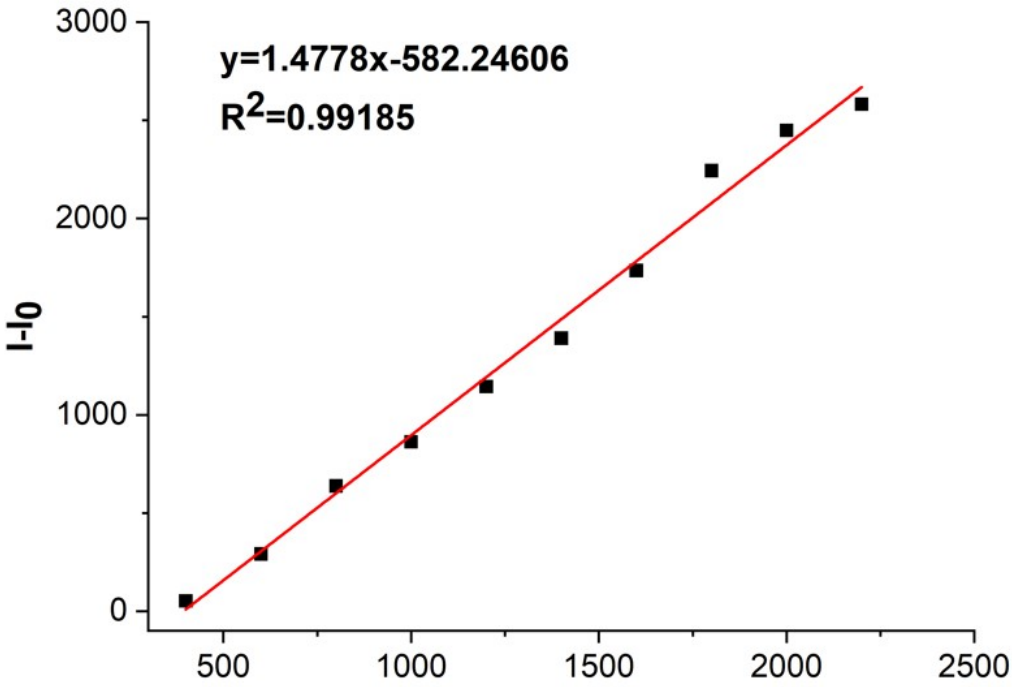

Fig. S27 Linear plot of the enhancement coefficients of **1a** suspensions for sensing of HSO_3^-.

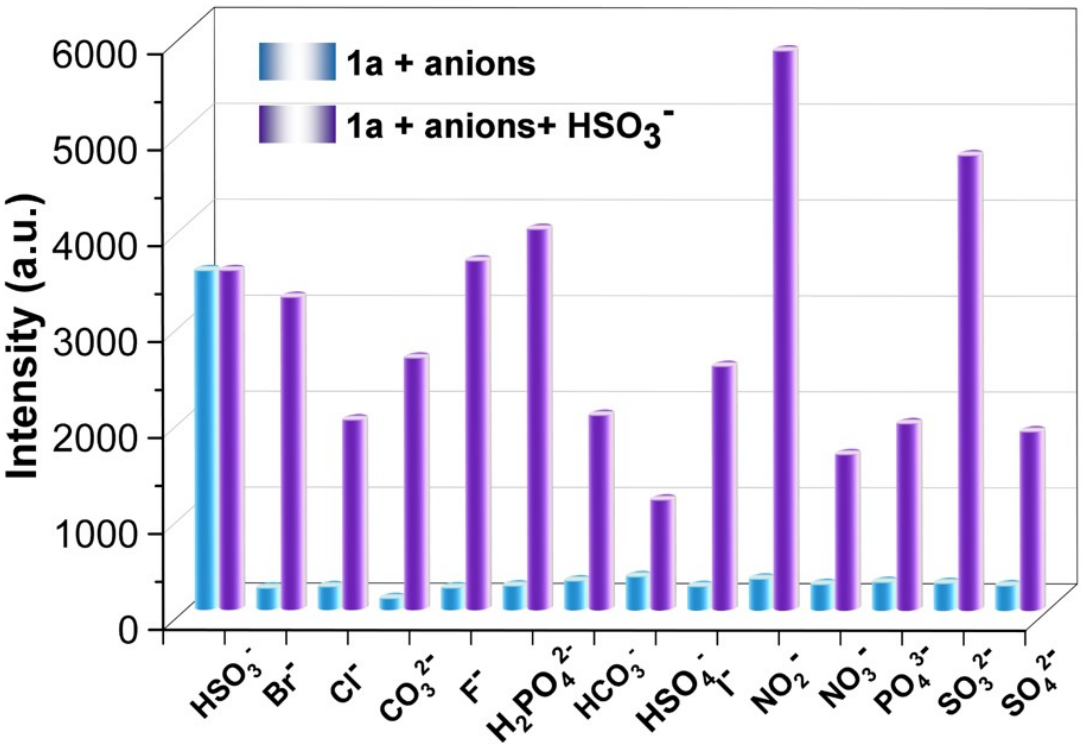

Fig. S28 Anti-interference ability of **1a** for luminescent sensing HSO_3^-

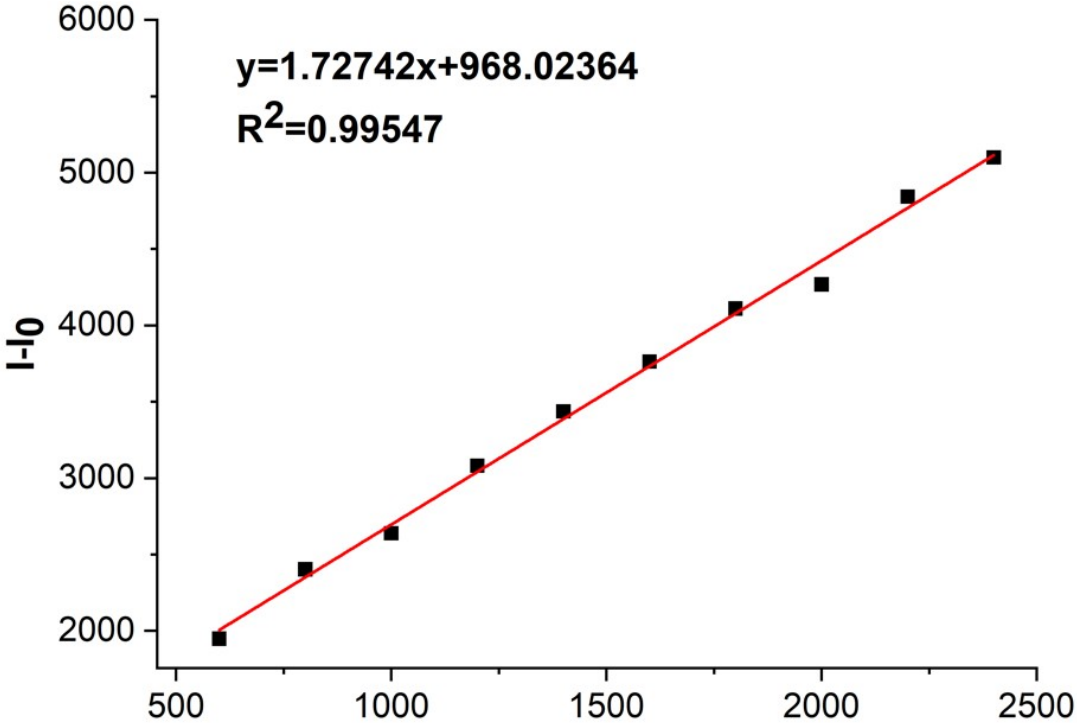

Fig. S29 Linear plot of the enhancement coefficients of **2a** suspensions for sensing of HSO_3^-.

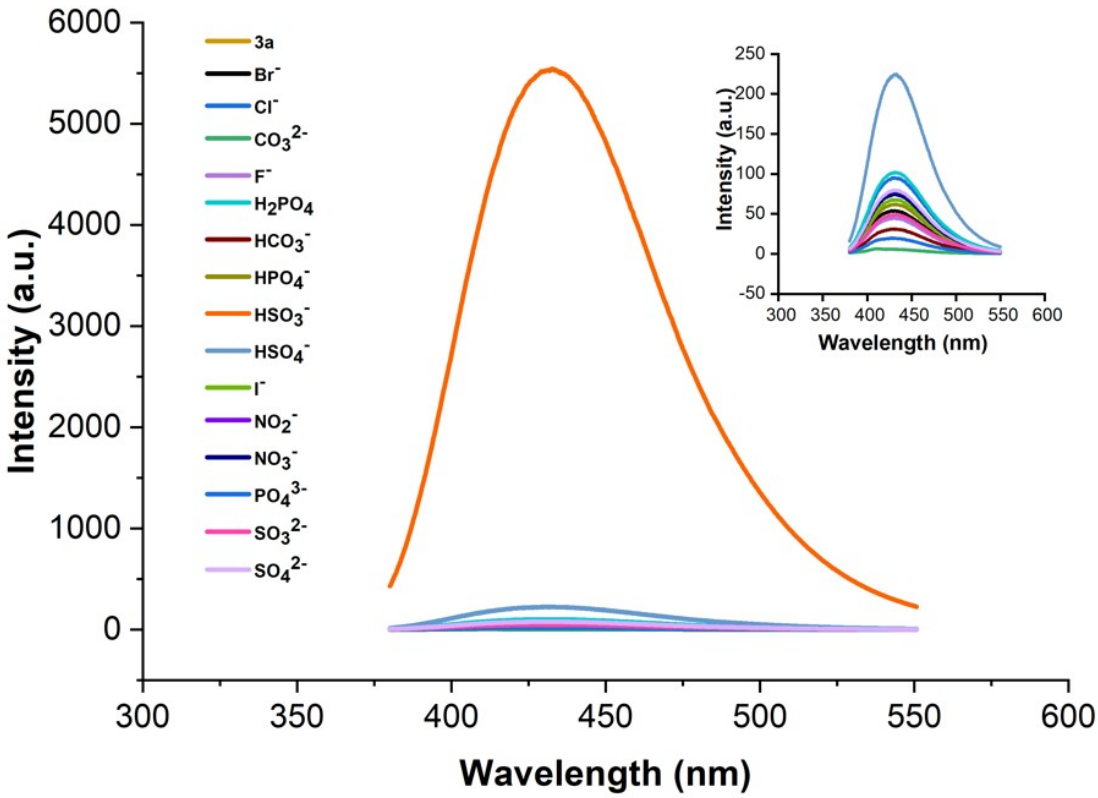

Fig. S30 Changes in fluorescent intensity for **3a** (1.0×10^{-5} M) in CH_3CN/H_2O (1:2, v/v) upon addition of different anions (Na^+ salts in H_2O).

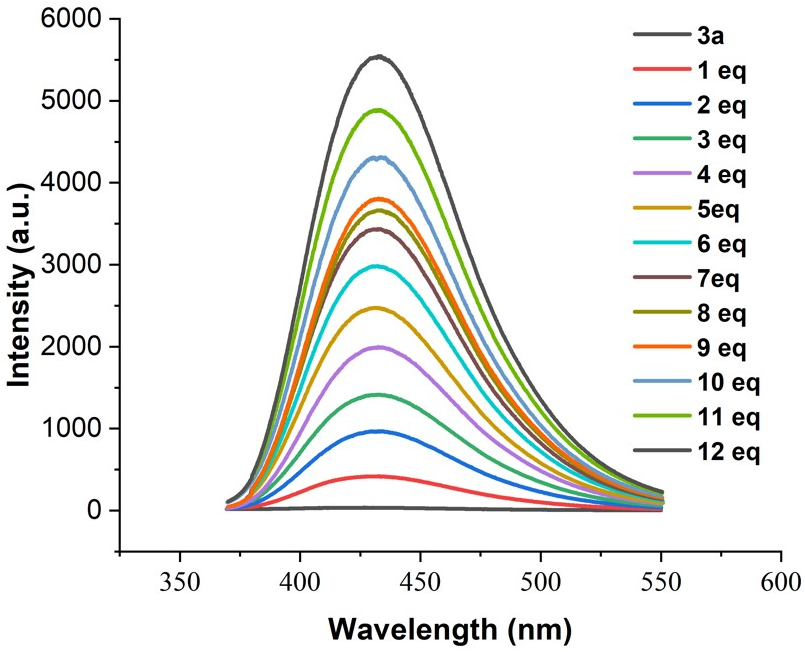

Fig. S31 Fluorescence spectra of **3a** in CH_3CN/H_2O ((1:2, v/v) for various concentrations of HSO_3^-.

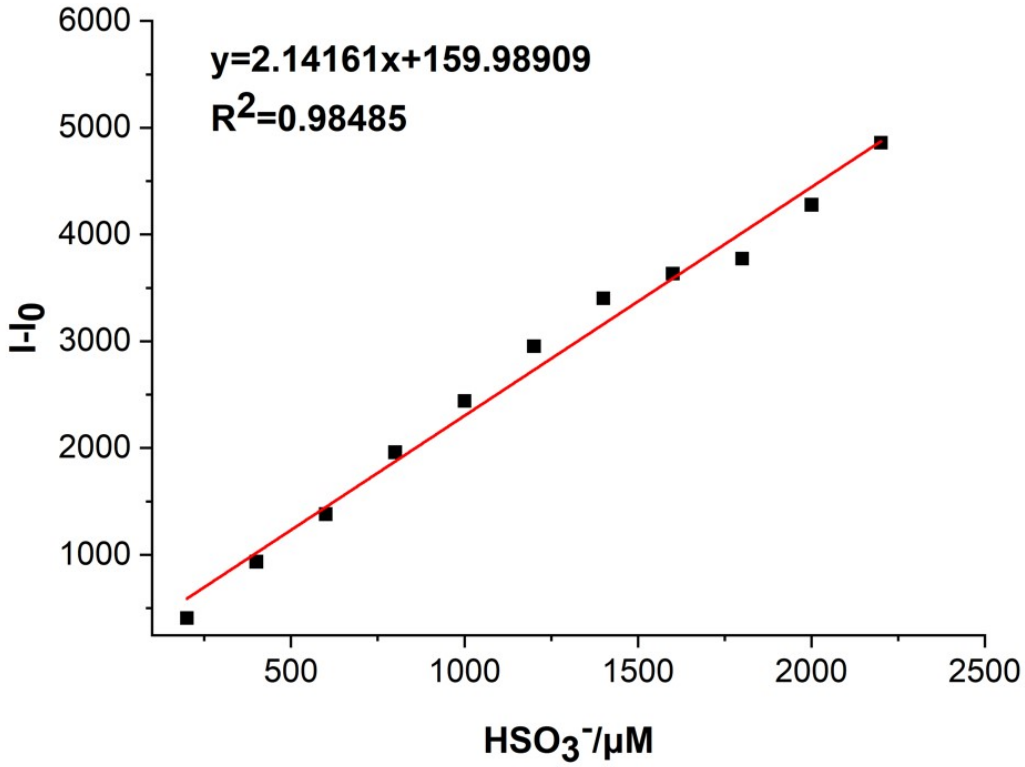

Fig. S32 Linear plot of the enhancement coefficients of **3a** suspensions for sensing of HSO_3^-.

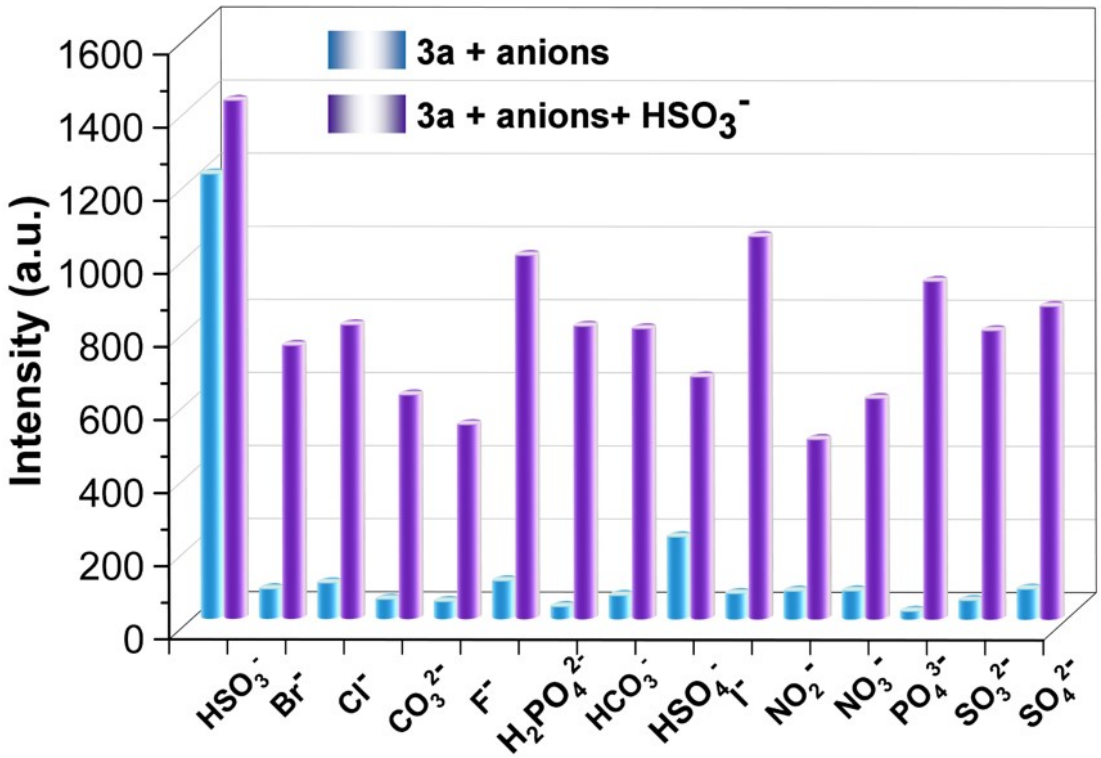

Fig. S33 Anti-interference ability of **3a** for luminescent sensing HSO_3^-

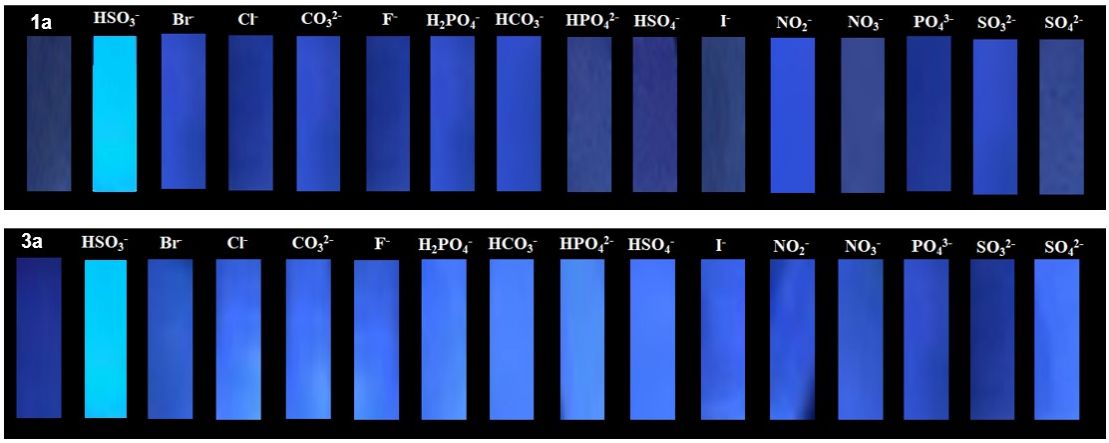

Fig. S34 Photographs of strips of the luminescent test paper of **1a** and **3a** after exposure to various anions under a UV lamp (λ_{ex} = 365 nm).

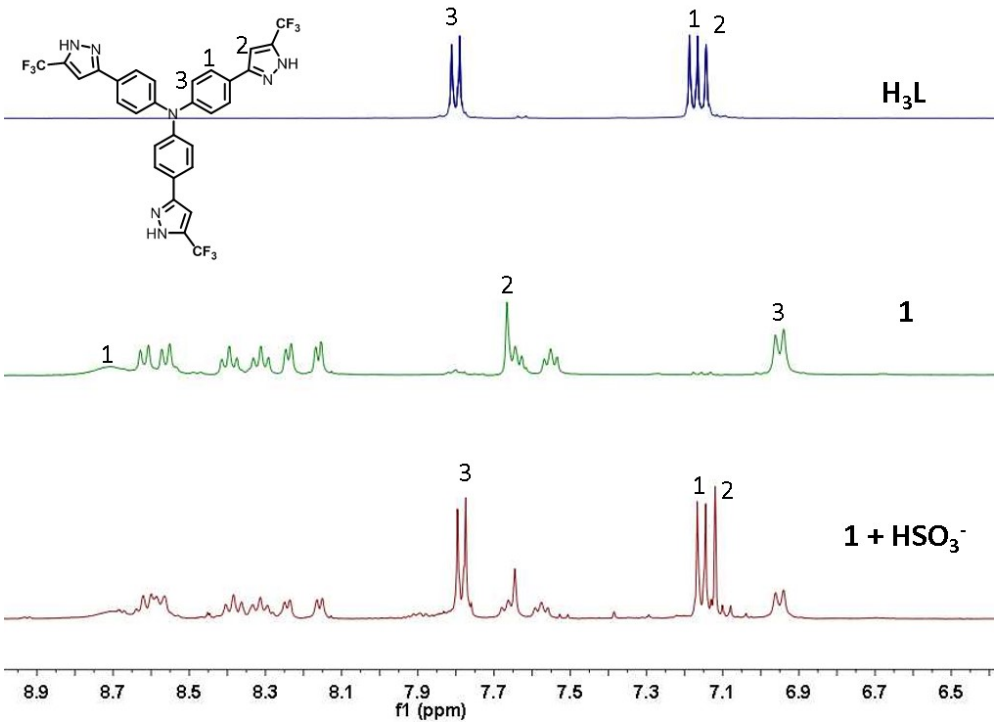

Fig. S35 ^{1}H NMR spectra of H_3L (a), **1** (b), **1** + $NaHSO_3$ (c) in DMSO-d_6.

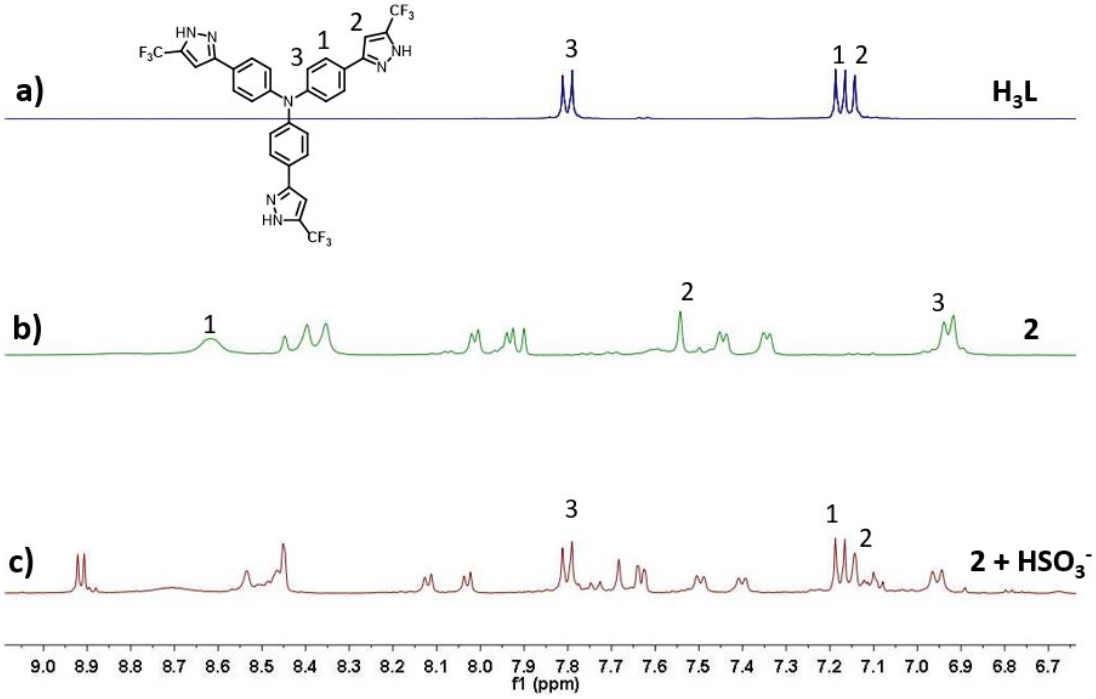

Fig S36 ^{1}H NMR spectra of H_3L (a), **2** (b), **2** + $NaHSO_3$ (c) in DMSO-d_6.

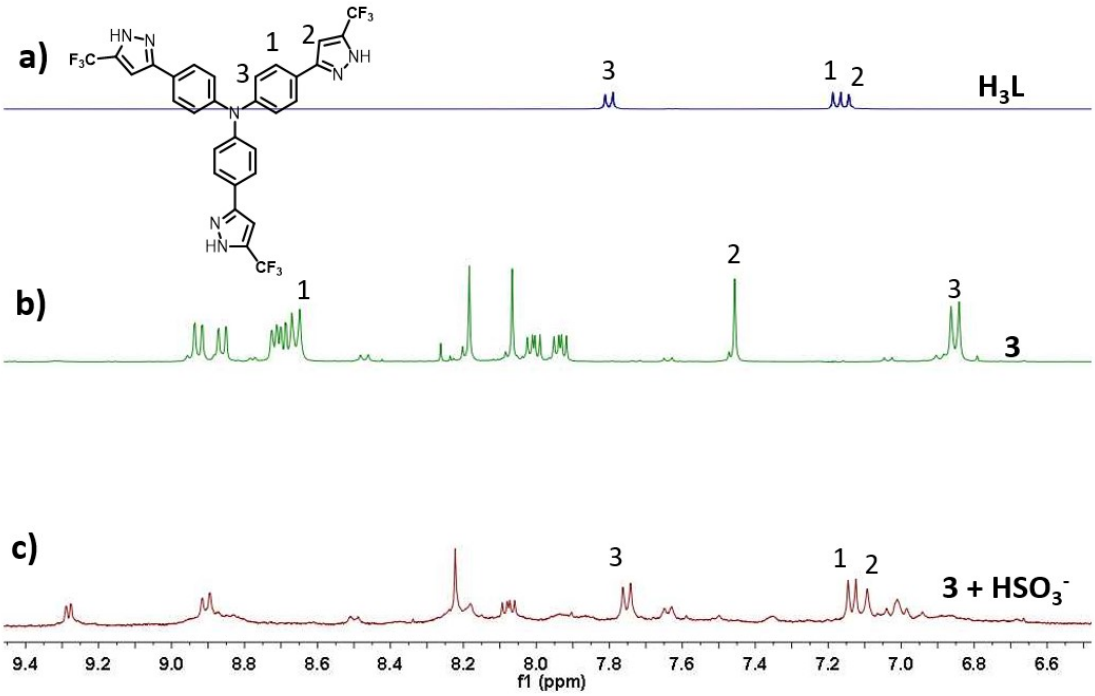

Fig. S37 ^{1}H NMR spectra of H_3L (a), **3** (b), **3** + $NaHSO_3$ (c) in DMSO-d_6.

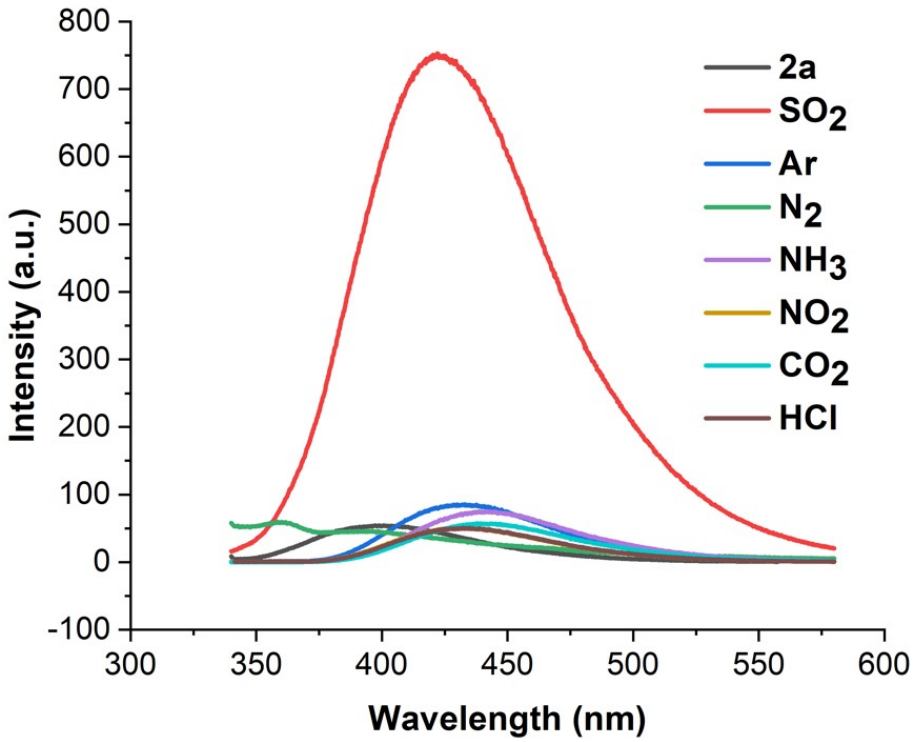

Fig. S38 Enhancement effect of various gas species on the fluorescence of **2a**.

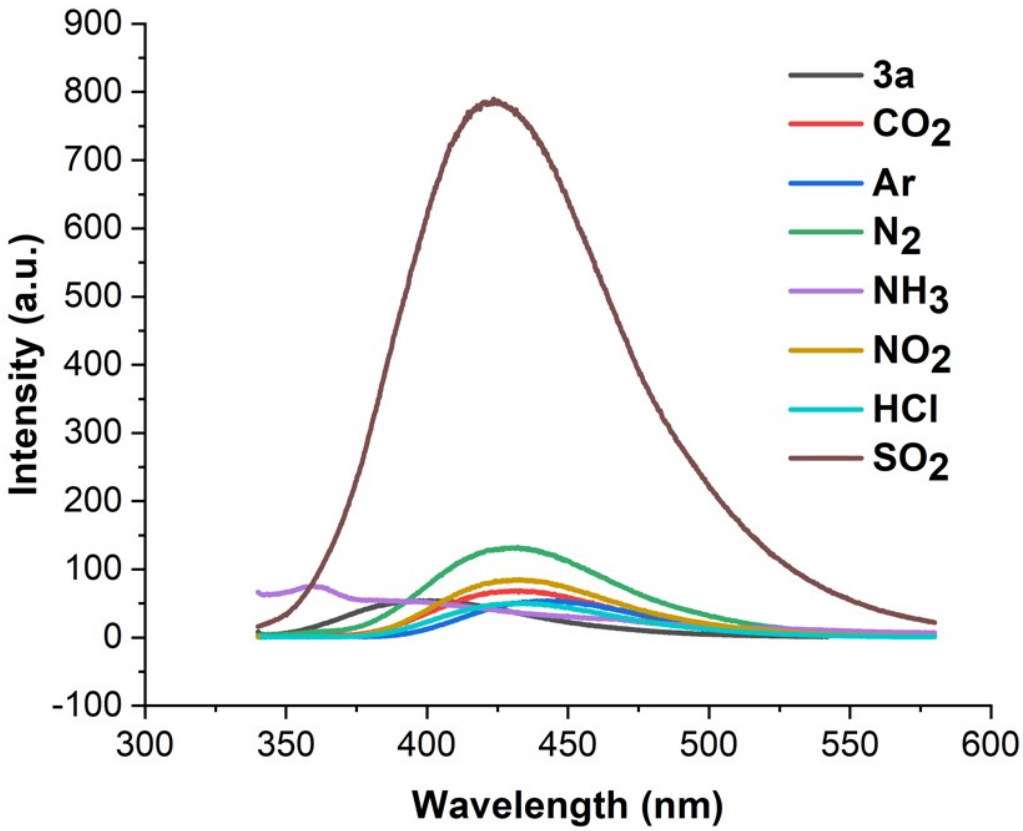

Fig. S39 Enhancement effect of various gas species on the fluorescence of **3a**.

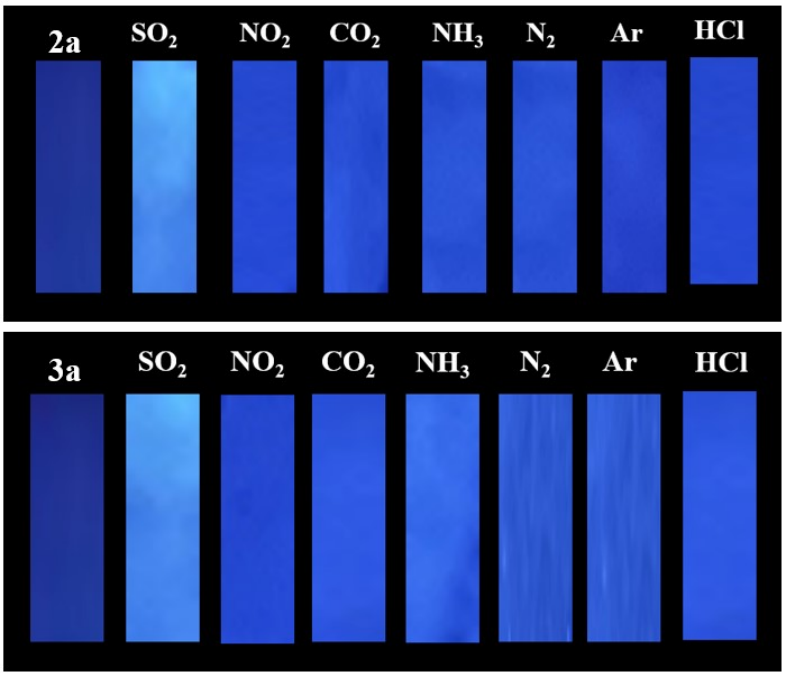

Fig. S40 Photographs of strips of the luminescent test paper of **2a** and **3a** after exposure to various gases under a UV lamp (λ_{ex} = 365 nm).

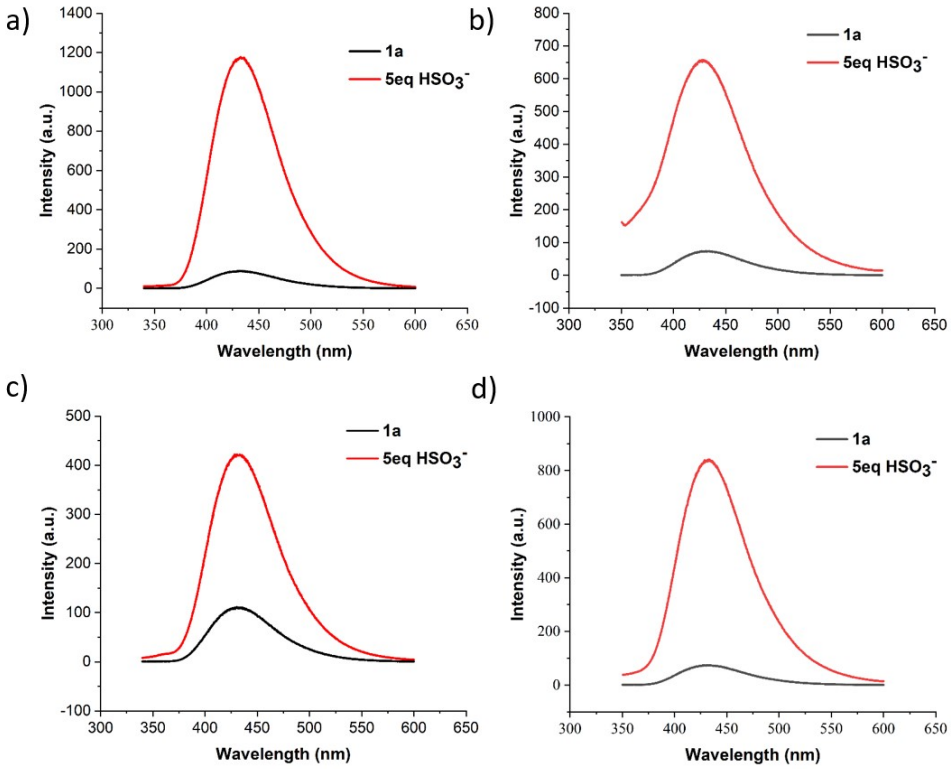

Fig. S41 Detection of HSO_3^- in practical water samples in **1a**: a) deionized water, b) tap water, c) sea-water, and d) lake water.

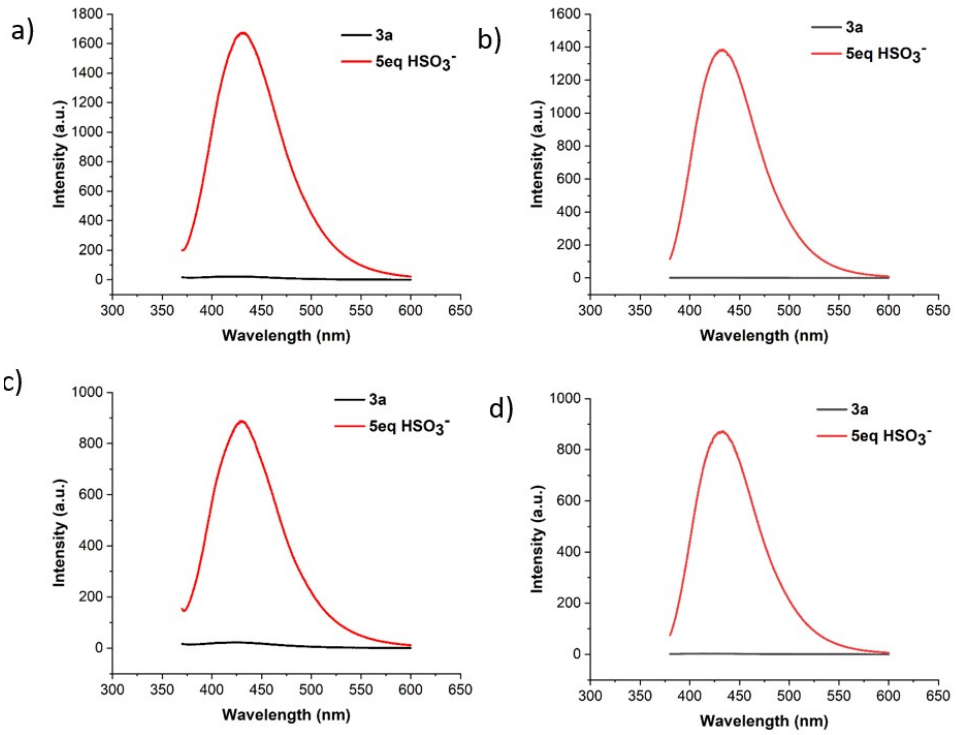

Fig. S42 Detection of HSO_3^- in practical water samples in **3a**: a) deionized water, b) tap water, c) sea-water, and d) lake water.

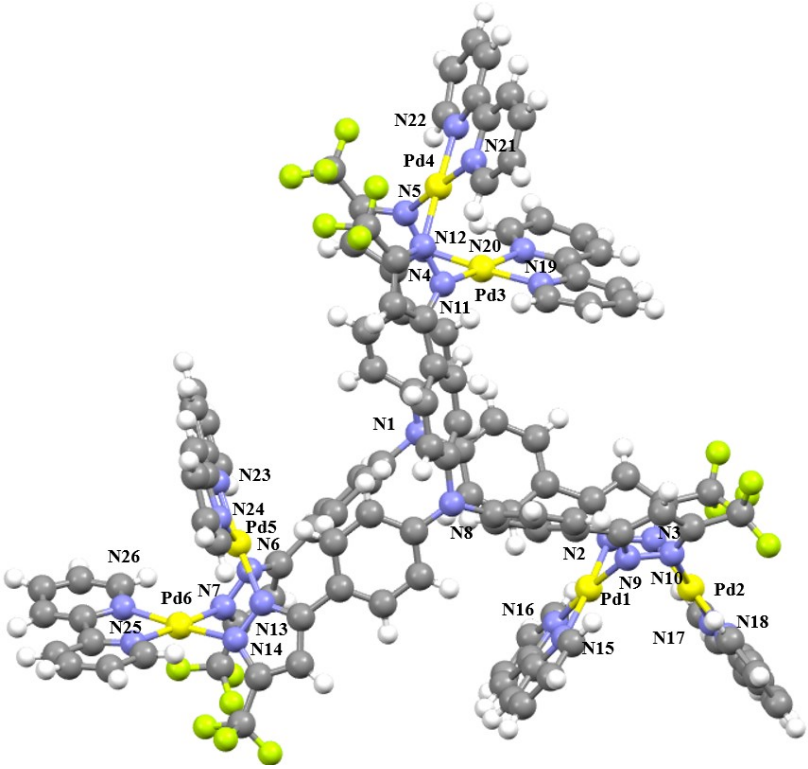

Fig. S43 Single crystal structures of **1**.

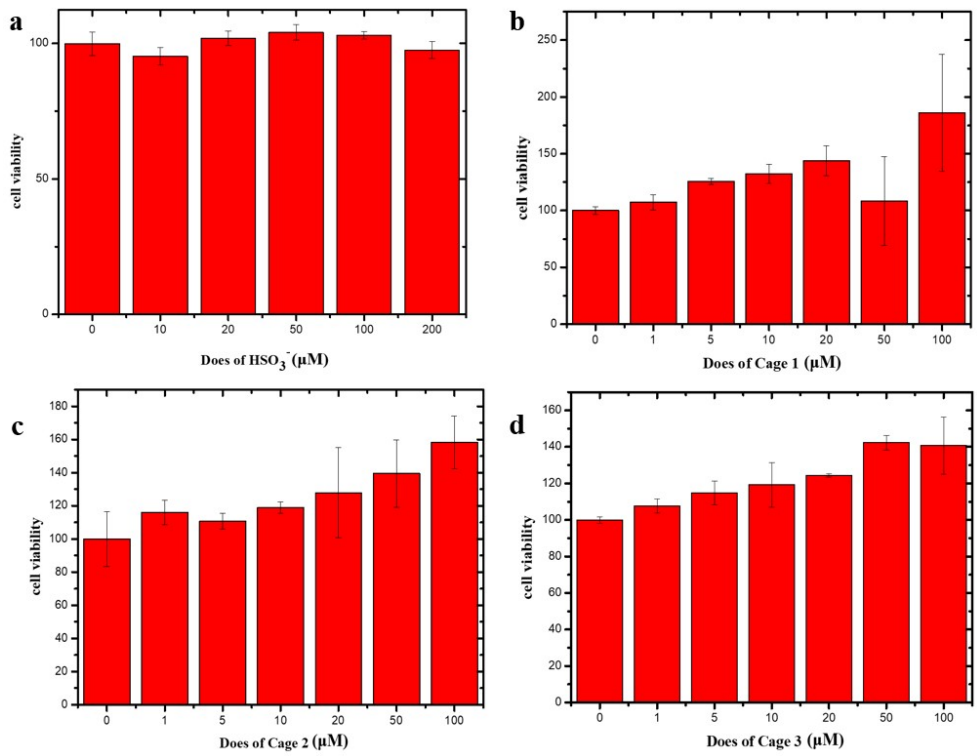

Fig. S44 Cytotoxicity test of HSO_3^-, **1a, 2a** and **3a** in Hela cells.

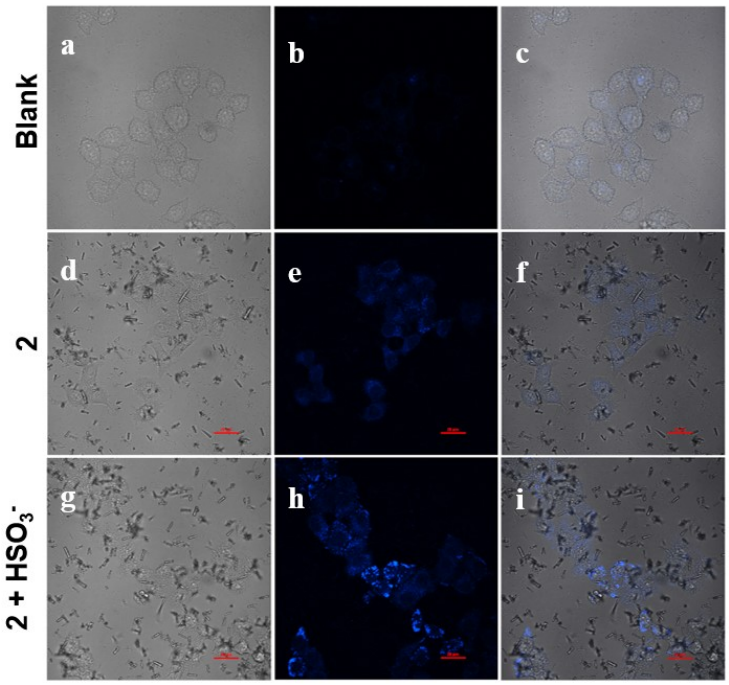

Fig. S45 Fluorescence images of HeLa cells incubated with or without probe **2a** (10 μM) and HSO_3^- (0 eq or12 eq); (a), (d) and (g) Bright field images;(b), (e) and (h) fluorescent images from the blue channel (from 429–474 nm) of laser scanning confocal microscope; (c), (f) and (i) Merge images.

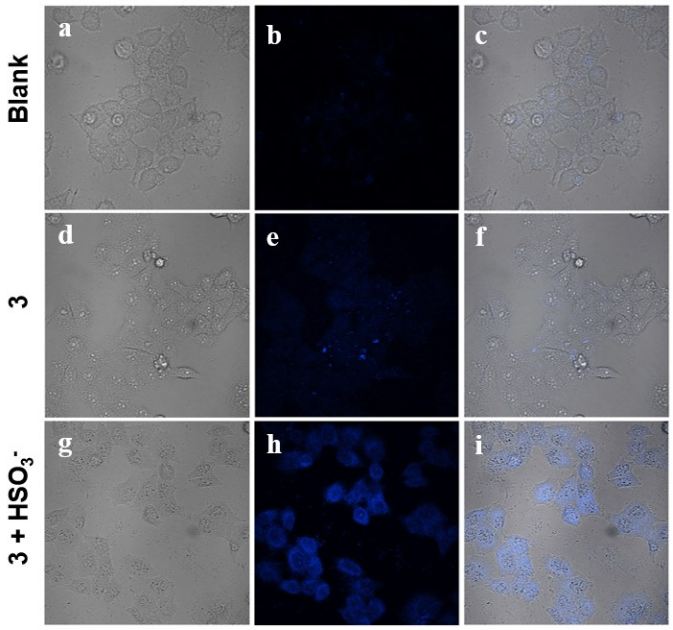

Fig. S46 Fluorescence images of HeLa cells incubated with or without probe **3a** (10 μM) and HSO_3^- (0 eq or12 eq); (a), (d) and (g) Bright field images;(b), (e) and (h) fluorescent images from the blue channel (from 429–474 nm) of laser scanning confocal microscope; (c), (f) and (i) Merge images.

Table S1 Crystallographic data for complexes $1{\cdot}6PF_6^-$

	$1{\cdot}6PF_6^-$
Formula	$C_{166}H_{198}F_{48}N_{26}O_{30}P_5Pd_6S_7$
FW	4967.16
crystal system	Monoclinic
space group	C12/a1
a [Å]	55.0704(4)
b [Å]	31.5923(2)
c [Å]	26.9571(2)
α [º]	90
β [º]	115.8350(10)
γ [º]	90
V [Å3]	42212.4(6)
Z	8
ρ calcd, [Mg/cm^3]	1.563
μ [mm^{-1}]	6.026
F(000)	20088
θ max	2.157 to 77.116
reflections collected	301265
Independent reflections	42932 []R(int)= 0.0588
goodness-of-fit on F^2	1.013
R_1,wR_2 [I>=2σ (I)]	R_1=0.1317, wR_2=0.3177
R_1,wR_2 [all data]	R_1=0.1395, wR_2=0.3255

Table S2. Selected bond distances (Å) and angles (°) of complex $1 \cdot 6PF_6^- \cdot$

Bond Dist.[Å]		Bond Dist.[Å]	
Pd(1)-N(2)	2.009(10)	Pd(5)-N(14)	2.009(10)
Pd(1)-N(9)	2.004(10)	Pd(5)-N(23)	2.001(8)
Pd(1)-N(15)	1.965(7)	Pd(5)-N(24)	2.001(11)
Pd(1)-N(16)	2.003(10)	Pd(6)-N(7)	2.029(10)
Pd(2)-N(3)	2.013(10)	Pd(6)-N(13)	2.019(9)
Pd(2)-N(10)	2.017(11)	Pd(6)-N(25)	2.020(9)
Pd(2)-N(17)	1.971(9)	Pd(6)-N(26)	2.011(9)
Pd(2)-N(18)	2.026(10)	N(4)-N(5)	1.328(11)
Pd(3)-N(4)	2.028(9)	N(13)-N(14)	1.369(11)
Pd(3)-N(20)	2.023(10)	N(6)-N(7)	1.364(11)
Pd(3)-N(19)	2.024(9)	N(9)-N(10)	1.320(12)
Pd(3)-N(12)	2.051(8)	N(11)-N(12)	1.317(11)
Pd(4)-N(5)	2.029(9)	N(2)-N(3)	1.385(11)
Pd(4)-N(11)	2.038(8)	Pd(1)-Pd(2)	3.0147(11)
Pd(4)-N(21)	2.009(7)	Pd(3)-Pd(4)	3.0896(10)
Pd(4)-N(22)	2.005(8)	Pd(5)-Pd(6)	3.0530(10)
Pd(5)-N(6)	2.009(12)		
Bond Angel[°]		Bond Angel[°]	
N(2)-Pd(1)-Pd(2)	66.7 (2)	N(21)-Pd(4)-Pd(3)	117.9(2)
N(9)-Pd(1)-Pd(2)	65.6(3)	N(21)-Pd(4)-N(5)	97.8(3)
N(9)-Pd(1)-N(2)	85.5(4)	N(21)-Pd(4)-N(11)	177.2(3)
N(15)-Pd(1)-Pd(2)	112.7(3)	N(22)-Pd(4)-Pd(3)	110.8(2)
N(15)-Pd(1)-N(2)	97.1(4)	N(22)-Pd(4)-N(5)	174.2(3)
N(15)-Pd(1)-N(9)	176.1(4)	N(22)-Pd(4)-(N11)	96.2(4)
N(15)-Pd(1)-N(16)	80.3(4)	N(22)-Pd(4)N-(21)	81.4(3)
N(16)-Pd(1)-Pd(2)	110.2(3)	N(6)-Pd(5)-Pd(6)	65.3(2)
N(16)-Pd(1)-N(2)	175.0(4)	N(14)-Pd(5)Pd-(6)	64.6(2)
N(16)-Pd(1)-N(9)	96.8(4)	N(14)-Pd(5)-N(6)	84.8(4)
N(3)-Pd(2)-Pd(1)	65.5(3)	N(23)-Pd(5)-Pd(6)	111.5(3)
N(3)-Pd(2)-N(10)	84.7(5)	N(23)-Pd(5)-N(6)	175.6(4)
N(3)-Pd(2)-N(18)	176.6(6)	N(23)-Pd(5)-N(14)	96.5(4)
N(10)-Pd(2)-Pd(1)	64.5(3)	N(23)-Pd(5)-N(24)	80.2(5)
N(10)-Pd(2)-N(18)	98.6(5)	N(24)-Pd(5)-Pd(6)	115.9(3)
N(17)-Pd(2)-N(3)	96.0(5)	N(24)-Pd(5)-N(6)	98.5(5)
N(17)-Pd(2)-N(10)	176.7(4)	N(24)-Pd(5)-N(14)	176.6(6)
N(17)-Pd(2)-N(18)	80.6(5)	N(7)-Pd(6)-Pd(5)	65.3(3)
N(17)-Pd(2)-Pd(1)	112.8(3)	N(13)-Pd(6)-Pd(5)	66.0(2)
N(18)-Pd(2)- Pd(1)	115.3(3)	N(13)-Pd(6)-N(7)	84.3(4)
N(4)-Pd(3)- Pd(4)	64.0(2)	N(13)-Pd(6)-N(25)	174.2(3)
N(4)-Pd(3)-N(12)	83.9(4)	N(25)-Pd(6)-Pd(5)	109.0(2)
N(12)-Pd(3)-Pd(4)	64.3(3)	N(25)-Pd(6)-N(7)	96.4(4)
N(19)-Pd(3)-Pd(4)	115.7(3)	N(26)-Pd(6)-Pd(5)	119.4(2)
N(19)-Pd(3)-N(4)	96.7(4)	N(26)-Pd(6)-N(7)	175.2(4)
N(19)-Pd(3)-N(12)	179.4(4)	N(26)-Pd(6)-N(13)	98.1(4)
N(20)-Pd(3)-Pd(4)	117.1(3)	N(26)-Pd(6)-N(25)	81.6(4)

N(20)-Pd(3)-N(4)	177.9(4)	
N(20)-Pd(3)-N(12)	98.2(4)	
N(20)-Pd(3)-N(19)	81.3(4)	
N(5)-Pd(4)-Pd(3)	64.4(2)	
N(5)-Pd(4)-N(11)	84.7(4)	
N(11)-Pd(4)-Pd(3)	64.2(2)	